Study of Deuteron Induced Transfer Reactions on ^{27}Al

By

VISHAL SRIVASTAVA
Enrolment No PHYS04201004005
Experimental Nuclear Physics Division
Variable Energy Cyclotron Centre, Kolkata, India

A thesis submitted to the
Board of Studies in **Physical Sciences**

In partial fulfillment of requirements
for the Degree of

DOCTOR OF PHILOSOPHY

of

HOMI BHABHA NATIONAL INSTITUTE
Bhabha Atomic Research Centre
Mumbai-400085, India

APRIL, 2016

Homi Bhabha National Institute

Recommendations of the Viva Voce Board

As members of the Viva Voce committee, we certify that we have read the dissertation prepared by **Vishal Srivastava** entitled "**Study of deuteron induced transfer reactions on ^{27}Al** " and recommend that it may be accepted as fulfilling the thesis requirement for the award of Degree of Doctor of Philosophy.

.....**Date:**
Chairman - Dr. Sudhee Ranjan Banerjee

.....**Date:**
Guide / Convener - Dr. Chandana Bhattacharya

.....**Date:**
Member 1 - Dr. Subinit Roy

.....**Date:**
Member 2 - Dr. Gopal Mukherjee

Final approval and acceptance of this dissertation is contingent upon the candidate's submission of the final copies of the thesis to HBNI.

I hereby certify that I have read this dissertation prepared under my direction and recommend that it may be accepted as fulfilling the thesis requirement.

Date:

Place:

Signature of Guide

Dr. Chandana Bhattacharya

STATEMENT BY AUTHOR

This dissertation has been submitted in partial fulfillment of requirements for an advanced degree at Homi Bhabha National Institute (HBNI) and is deposited in the Library to be made available to borrowers under rules of the HBNI.

Brief quotation from this dissertation are allowable without special permission, provided that accurate acknowledgement of source is made. Requests for permission for extended quotation from or reproduction of this manuscript in whole or in part may be granted by the Competent Authority of HBNI when in his or her judgement the proposed use of the material is in the interests of scholarship. In all other instances, however, permission must be obtained from the author.

Vishal Srivastava

DECLARATION

I, hereby declare that the investigation presented in the thesis has been carried out by me. The work is original and has not been submitted earlier as a whole or in part for a degree/diploma at this or any other Institution / University.

Vishal Srivastava

Publication list

Publications relevant to the thesis:

Referred Journals:

1. *"Experimental study of ^{26}Al through the 1n pick up reaction ^{27}Al(d,t)"*:
   Vishal Srivastava, C. Bhattacharya, T. K. Rana, S. Manna, S. Kundu, S. Bhattacharya, K. Banerjee, P. Roy, R. Pandey, G. Mukherjee, T.K. Ghosh, J. K. Meena, T. Roy, A. Chaudhuri, M. Sinha, A. Saha A. Dey, Md. A. Asgar, Subinit. Roy, and Md. M. Shaikh. Phys. Rev. C **91**, 054611 (2015).

2. *"Experimental investigation of T = 1 analog states of ^{26}Al and ^{26}Mg"*:
   Vishal Srivastava, C. Bhattacharya, T. K. Rana, S. Manna, S. Kundu, S. Bhattacharya, K. Banerjee, P. Roy, R. Pandey, G. Mukherjee, T.K. Ghosh, J. K. Meena, T. Roy, A. Chaudhuri, M. Sinha, A. Saha A. Dey, Md. A. Asgar, Subinit. Roy, and Md. M. Shaikh. Phys. Rev. C **93**, 044601 (2016).

3. *"Study of ^{26}Mg through the 1p pick up reaction ^{27}Al(d,^{3}He)"*:
   Vishal Srivastava, C. Bhattacharya, T. K. Rana, S. Manna, S. Kundu, S. Bhattacharya, K. Banerjee, P. Roy, R. Pandey, G. Mukherjee, T.K. Ghosh, J. K. Meena, T. Roy, A. Chaudhuri, M. Sinha, A. Saha A. Dey, Md. A. Asgar, Subinit. Roy, and Md. M. Shaikh. **arXiv:1510.04416.**

4. *"Structure of ^{26}Al studied by one -nucleon transfer reaction ^{27}Al(d,t)"*:
   Vishal Srivastava, C. Bhattacharya, T. K. Rana, S. Manna, S. Kundu, S. Bhattacharya, K. Banerjee, P.Roy, R. Pandey, G. Mukherjee, T. K. Ghosh, J. K. Meena, T. Roy, A. Chaudhuri, M. Sinha, A. Saha A. Dey, Md. A. Asgar, Subinit. Roy, and Md. M. Shaikh. EPJ Web of Conferences **86**, 00055 (2015).

5. *"Excited states of ^{26}Al studied via the reaction ^{27}Al(d,t)"*:
   Vishal Srivastava, C. Bhattacharya, T.K. Rana, S. Manna, S. Kundu, S. Bhattacharya, K. Banerjee, P. Roy, R. Pandey, G. Mukherjee, T.K. Ghosh, J.K.

Meena, T. Roy, A. Chaudhuri, M. Sinha, A. K. Saha, Md. A. Asgar, A. Dey, Subinit Roy, and Md. Moin Shaikh. Proceedings of NN2015 conference to be published in EPJ Web of Conferences (Accepted; in press).

Conference Proceedings:

1. *"Study of one neutron pick-up reaction $^{27}Al(d,t)$"*:
   Vishal Srivastava, C. Bhattacharya, T.K. Rana, S. Manna, S. Kundu, S. Bhattacharya, K. Banerjee, P. Roy, R. Pandey, G. Mukherjee, T.K. Ghosh, J.K. Meena, T. Roy, A. Chaudhuri, M. Sinha, A. Saha, Md. A. Asgar, A. Dey, Subinit Roy, and Md. Moin Shaikh. Proceedings of the DAE Symp. on Nucl. Phys. **59**, 358 (2014).

2. *"Study of one proton pick-up reaction $^{27}Al(d,^{3}He)$"*:
   Vishal Srivastava, C. Bhattacharya, T.K. Rana, S. Manna, S. Kundu, S. Bhattacharya, K. Banerjee, P. Roy, R. Pandey, G. Mukherjee, T.K. Ghosh, J.K. Meena, T. Roy, A. Chaudhuri, M. Sinha, A. Saha, Md. A. Asgar, A. Dey, Subinit Roy, and Md. Moin Shaikh. Proceedings of the DAE Symp. on Nucl. Phys. **60**, 342 (2015).

Other publications:

Referred Journals:

1. *"Fragment emission studies in low energy light ion reactions"*: T. K. Rana, C. Bhattacharya, S. Manna, **V. Srivastava**, K. Banerjee, S. Kundu, P. Roy, R. Pandey, A. Chaudhuri, T. Roy, T.K. Ghosh, G. Mukherjee, S. Bhattacharya, J.K. Meena, S. K. Pandit, K. Mahata, P. Patale, A. Shrivastava, and V. Nanal. EPJ Web of Conferences **86**, 00036 (2015).

2. *" Direct evidence of washing out of nuclear shell effects"*: A. Chaudhuri, T. K. Ghosh, K. Banerjee, S. Bhattacharya, Jhilam Sadhukhan, C. Bhattacharya, S.

Kundu, J. K. Meena, G. Mukherjee, R. Pandey, T. K. Rana, P. Roy, T. Roy, **V. Srivastava**, and P. Bhattacharya. Phys. Rev. C **91**, 044620 (2015).

3. *"Angular momentum dependence of the nuclear level density in the A170-200 Region"*: M. Gohil, Pratap Roy, K. Banerjee, C. Bhattacharya, S. Kundu, T. K. Rana, T. K. Ghosh, G. Mukherjee, R. Pandey, H. Pai, **V. Srivastava**, J. K. Meena, S. R. Banerjee, S. Mukhopadhyay, D. Pandit, S. Pal, and S. Bhattacharya. Phys. Rev. C **91**, 014609 (2015).

4. *"No influence of a N=126 neutron-shell closure in fission-fragment mass distributions"*: A. Chaudhuri, T. K. Ghosh, K. Banerjee, S. Bhattacharya, Jhilam Sadhukhan, C. Bhattacharya, S. Kundu, J. K. Meena, G. Mukherjee, R. Pandey, T. K. Rana, P. Roy, T. Roy, **V. Srivastava**, and P. Bhattacharya. Phys. Rev. C **92**, 041601(R) (2015).

5. *"Fusion - fission dynamics studies using mass distribution as a probe"*: T K Ghosh,A Chaudhuri, K. Banerjee, S. Bhattacharya, C. Bhattacharya, ,S Kundu, G. Mukherjee, R Pandey, T K Rana, P Roy, T Roy, **V Sristava**, P.Bhattacharya. Pramana Journal of Physics **85**, 291-301(2015).

6. *"Further limit on 3α decay of Hoyle state"*: T. K. Rana, C. Bhattacharya, S. Bhattacharya, S. Kundu, K. Banerjee, T. K. Ghosh, G. Mukherjee, R. Pandey, P. Roy, **V. Srivastava**, M. Gohil, J. K. Meena, H. Pai, A. K. Saha, J. K. Sahoo, and R. M. Saha. EPJ Web of Conferences, **66**, 03072 (2014).

7. *"Angular momentum dependence of the nuclear level density parameter"*: M. Gohil, Pratap Roy, K. Banerjee, S. Bhattacharya, C. Bhattacharya, S. Kundu, T. K. Rana, T. K. Ghosh, G. Mukherjee, R. Pandey, J. K. Meena, H. Pai, **V. Srivastava**, A. Dey, Deepak Pandit, S. Mukhopadhyay, S. Pal, and S. R. Banerjee. EPJ Web of Conferences, **66**, 03073 (2014).

8. *"Estimation of direct components of the decay of the Hoyle state"*: T. K. Rana, S. Bhattacharya, C. Bhattacharya, S. Kundu, K. Banerjee, T. K. Ghosh, G. Mukher-

jee, R. Pandey, P. Roy, **V. Srivastava**, M. Gohil, J. K. Meena, H. Pai, A. K. Saha, J. K. Sahoo, and R. M. Saha. Phys. Rev. C **88**, 021601(R) (2013).

9. *"Effect of collectivity on the nuclear level density"*: Pratap Roy, K. Banerjee, M. Gohil, C. Bhattacharya, S. Kundu, T. K. Rana, T. K. Ghosh, G. Mukherjee, R. Pandey, H. Pai, **V. Srivastava**, J. K. Meena, S. R. Banerjee, S. Mukhopadhyay, D. Pandit, S. Pal, and S. Bhattacharya. Phys. Rev. C **88**, 031601(R) (2013).

10. *"Angular-momentum-gated light-particle evaporation spectra from $^{97}Tc^{*}$ and $^{62}Zn^{*}$ systems"*: Pratap Roy, K. Banerjee, S. Bhattacharya, C. Bhattacharya, S. Kundu, T. K. Rana, T. K. Ghosh, G. Mukherjee, R. Pandey, J. K. Meena, M. Gohil, H. Pai, **V. Srivastava**, A. Dey, Deepak Pandit, S. Mukhopadhyay, S. Pal, and S. R. Banerjee. Phys. Rev. C **86**, 044622 (2012).

Conferences/Symposiums:

1. *"Inelastic scattering of alpha particles from ^{27}Al target"*: Aparajita Dey, V. Srivastava, S. Ganguly, C. Bhattacharya, T.K. Rana, S. Kundu, K. Banerjee, P. Roy, H. Pai, T.K. Ghosh, R. Pandey, G. Mukherjee ,J.K. Meena, M.R. Gohil, and S.Bhattacharya. Proceedings of the DAE Symp. on Nucl. Phys. **60**, 350 (2015).

2. *"Fragment emission mechanism in $^{12,13}C$ + ^{12}C reactions"*: S. Manna,C. Bhattacharya,T.K. Rana,**V. Srivastava**,K. Banerjee,S. Kundu,P. Roy,R. Pan dey, A. Chaudhury,T. Roy,T.K. Ghosh,G. Mukherjee,S. Bhattacharya,J.K. Meena,S.K. Pandit ,K. M hata,P. Patale,A. Shrivastava,V. Nanal,S. Pal. Proceedings of the DAE Symp. on Nucl. Phys. **59**, 560 (2014).

3. *"Elastic Scattering of alpha particles from ^{28}Si target"*: Aparajita Dey, S.Ganguli, **V. Srivastava**, T.K.Rana, S.Kundu, K.Banerjee, H.Pai, C.Bhattacharya, T.K.Ghosh, R.Pandey, G.Mukherjee, J.K.Meena, M.R.Gohil, S. Bhattacharya. Proc. of DAE- BRNS symposium on Nucl. Phys. Vol. **57**, 472 (2014).

4. *"Shell effects in fission fragment mass distribution"*: A. Chaudhuri, T.K. Ghosh, K. Banerjee, S. Bhattacharya, C. Bhattacharya, S.Kundu, J. K. Meena, G. Mukherjee, R. Pandey, T. K. Rana, P. Roy, T.Roy, **V. Srivastava**, A. Saha, R. SahaMondal, J. K. Sahoo, and P. Bhattacharya. Book of Abstracts, Page 21, FUSION14, February 24-28, 2014, Inter University Accelerator Centre, New Delhi, India.

5. *"Study of fragment emission in* $^{32}S+^{12}C$ *reaction"*: R Pandey, C Bhattacharya, S Kundu, K. Banerjee, S Manna,T. K Rana, J.K Meena, T Roy, A. Chaudhauri, Md A. Asgar, **V. Srivastava**, A Dey, M Sinha,G Mukherjee,P Roy,T.K Ghosh,S. Bhattacharya, A Srivastava, K Mahata, S. K. Pandit, P Patle, S Pal, V Nanhal. Proc. of DAE symposium on Nucl. Phys. Vol. **59**, 614 (2014).

6. *"Shell effects in fission fragment mass distributions"*: A Chaudhuri, T. K Ghosh, K Banerjee, S Bhattacharya,C Bhattacharya, S Kundu, J. K Meena, R Mondal Saha, G Mukherjee, R Pandey, T. K. Rana, P Roy, T Roy, A. K.Saha, J. K Sahoo,**V. Srivastava**, P Bhattacharya. Proc. of DAE symposium on Nucl. Phys. Vol. **59**, 478 (2014).

7. *"Characterization of a segmented clover detector"*: Md. Ali Asgar, Tanmoy Roy, Gopal Mukherjee, Soumik Bhattacharya, Abhirup Chaudhuri, **Vishal Srivastava**, Sarmishtha Bhattacharyya, Sailajananda Bhattacharya, Chan dana Bhattacharya, Tilak Kumar Ghosh, Kaushik Banerjee, Samir Kundu, Ratnesh Pan dey, Tapan Kumar Rana, Pratap Roy, Santu Manna, Jayanta Kumar Sahoo, Jaikiran Meena,Amiya Kumar Saha,Ruchismita Mondal Saha, Pulak Mukhopadhyay,Anindita Choudhury, Imran Shaik. Proc. of DAE symposium on Nucl. Phys. Vol.**59**, 882 (2014).

8. *"Isotopic effects in fragment emission studies in low energy light ion reactions"*: C Bhattacharya, T. K. Rana, Santu Manna, **V. Srivastava**, K Banerjee, S Kundu, P Roy, R Pandey, A Chaudhuri, T Roy, T K Ghosh, G Mukherjee, S Bhattacharya, J K Meena, S K Pandit, K Mahata, P Patale, A Shrivastava,V Nanal.

Proceedings of the DAE International symposium on Nuclear Physics, BARC, Mumbai, India, Vol. **58**, 530 (2013).

9. *"Study of (^{4}He, t) reaction on ^{27}Al target at 50 MeV"*: Aparajita Dey, **Vishal Srivastava**, C. Bhattacharya, S. Ganguly, T. K. Rana, S. Kundu1, T. K. Ghosh, K. Banerjee, P. Roy, R. Pandey, H. Pai, G. Mukherjee , M.R. Gohil , J.K. Meena, S. Bhattacharya. Proceedings of the DAE International symposium on Nuclear Physics, BARC, Mumbai, India, Vol. **58**, 594 (2013).

10. *"Signature of collective enhancement in nuclear level density"*: Pratap Roy, K. Banerjee, M. Gohil, C. Bhattacharya, S. Kundu, T. K. Rana, T. K. Ghosh, G. Mukherjee, R. Pandey, H. Pai, **V. Srivastava**, J. K. Meena, S. R. Banerjee, S. Mukhopadhyay, D. Pandit, S. Pal, S. Bhattacharya. Proceedings of the DAE International symposium on Nuclear Physics, BARC, Mumbai, India, Vol. **58**, 378 (2013).

11. *"Measurement of efficiency and time resolution of PPAC"*: R. Pandey, T. K Ghosh, K. Banerjee, P. Roy, C. Bhattacharya, A. Chaudhuri, S. Kundu, T. K. Rana, G. Mukherjee, J. K. Meena, **V. Srivastava**, A. K. Saha, J. K. Sahoo, S. Bhattacharya. Proceedings of the DAE International symposium on Nuclear Physics, BARC, Mumbai, India, Vol. **58**, 982 (2013).

12. *"Elastic Scattering of alpha particles from ^{27}Al target"*: Aparajita Dey, S. Ganguli, **V. Srivastava**, T. K. Rana, S. Kundu, K. Banerjee, H. Pai, C. Bhattacharya, T. K. Ghosh, R. Pandey, G. Mukherjee, J. K. Meena, M. R. Gohil, S. Bhattacharya. Proc. of DAE- BRNS symposium on Nucl. Phys. Vol. **57**, 438 (2012).

13. *"(α,^{3}He) and (α,^{3}H) transfer reaction studies at E_α=60 MeV"*:
R. Pandey, A. Dey, T. K. Rana, M. Biswas, T. K .Ghosh, C. Bhattacharya, S. Kundu, K. Ban erjee, G. Mukherjee, P. Roy, J. K. Meena, **V. Srivastava**, H. Pai, M. Gohil, S. Bhattacharya. Proc. of DAE- BRNS symposium on Nucl. Phys. Vol. **57**, 526 (2012).

14. *"Study of angular momentum gated light-particle evaporation spectra in ^{4}He + ^{93}Nb and ^{4}He + ^{58}Ni reactions"*: Pratap Roy, K. Banerjee, S. Kundu, T. K. Rana, T. K. Ghosh, C. Bhattacharya, G. Mukherjee, R. Pandey, J. K. Meena, M. Gohil, H. Pai, **V. Srivastava**, A. Dey, S. Mukhopadhyay, D. Pan dit, S. Pal, S. R. Banerjee, and S. Bhattacharya. Proc. of DAE- BRNS Symposium on Nucl. Phys. Vol. **57**, 420 (2012).

15. *"Charged particle detector array: 450-1750"*: S. Kundu, C. Bhattacharya, T. K. Rana, K. Banerjee, S. Bhattacharya, J. K. Meena, R. Saha, G. Mukherjee, T. K. Ghosh, R. Pandey, P. Roy, M. Gohil, **V. Srivastava**, A. Dey, G. Pal, S. Roy, S. R. Bajirao, C. Nandi. Proc. of DAE symposium on Nucl. Phys. Vol.**57**, 86 (2012).

16. *"Development of a low pressure PPAC for detection of heavy charged particles"*: R. Pandey, T. K. Ghosh, J. K. Meena, K. Banerjee, C. Bhattacharya, S. Bhattacharya, M. Gohil, G. Mukherjee, S. Kundu, T. K. Rana, P. Roy, H. Pai, **V. Srivastava**. Proc. of DAE symposium on Nucl. Phys. Vol. **57**, 930 (2012).

Dedicated To My Parents

Acknowledgements

First, I would like to thanks to my supervisor, Prof. Chandana Bhattacharya and gratefully acknowledge her for valuable guidance, encouragement, motivation and for personally supporting me throughout my Ph.D work. I am extremely fortunate to have Prof. Chandana Bhattacharya as my guide. Personal note"Madam, you have shown your faith in me, encouraged me and guided me, I thank you from depth of my heart for being my supervisor and for care like a family member".

Apart from her, I would like to thank to the members of my Thesis advisory committee: Prof. S. R. Banerjee (Head, Experimental Physics Group, VECC), Prof. Subinit Roy and Dr. Gopal Mukherjee, for their valuable advices and comments.

Apart from the members of my Thesis advisory committee, I am extremely thankful to Prof. Sailajananda Bhattacharya for his continuous support, discussions and encouragement during my Phd tenure which I needed to complete my Thesis work, Thank you very much 'Sir'. I would also like to acknowledge my sincere thanks to my colleagues named as Dr. T. K. Rana, Dr. Samir Kundu, Ratnesh Pandey, Dr. Kauhik Banerjee, Dr. T. K. Ghosh, P. Roy, Jaikiran Meena, Santu Manna, Dr. Mandira Sinha, Dr. Aparajita Dey, Abhirup Chauduri, Tanmoy Roy, Md. Ali Asgar, R. Saha Modal, A. K. Saha and Jayanta Sahu who had helped me to perform my experiment and made significant discussion regarding the present thesis work.

I extremely grateful to Director, VECC, Prof. D. K. Srivastava, for providing a good research environment in VECC. I am thankful to him for motivating and encouraging me to do nuclear physics. I would also like to thank to my other senior colleagues Dr. Supriyo Mukhopadhyay, Dr. Deepak Pandit, Dr. Surajit Pal, Dr. S.C.L. Srivastava, Swagato Malik, Ashif Reza, Arindam Sikdar, Sujoy Chatterjee, Saurabh Srivastava, Hemendra Kumar pandey, Dr. Anand Kr. Dubey, Dr. Rupa Chaterjee and others from physics group, VECC, Kolkata.

I would like to give thanks to the members of the target making laboratory at VECC and to the operating staffs of the K130 Cyclotron to provide smooth and uninterrupted beams.

I would also like to give my special thanks to my colleagues from my batch Balaram Dey, Rihan, Shubhikash, Arindam, Sumit, Maitreyee and Sanoar for being good friends and their support. I am also very much thankful to my seniors from research scholar wing named as Haridas da, N. R. Sahoo, M. R. Gohil, S. K. Das, V. Roy, T. Bhattacharya, Abhishek Mishra, Surashree majumdar, Sukanya Mitra, Amal Giri, Payal Mohanti, Umme Jamil, Somnath Dey, Md. Nasim, Subhash Singha and other seniors for their inspiration and support and also to my juniors Somnath, Debojit, Arunabha, Noor and others for their support.

I am very much thankful to my dear friends Mithlesh Kumar Srivastava, Vikas Srivastava, Ankur Kumar Srivastava, Nitesh Kumar Srivastava, Chandra Dev Tripathi, Ashwani Kumar Shukla, Ravi Srivastava, Prem Narayan Pathak, Tushar Pradhan, Vijay Raj Sharma, Shailesh singh, Priya Sharma, bhoomika Maheshwari, Anukul dahl, Aman, Surendra, Shushil and others for for their priceless support. I am also grateful to all of my teachers including all teachers from my childhood to till present date, friends and seniors who have supported and inspired me all the times in my life. I am heartly thankfull to them.

Finally, I would like to thank my father and mother for their priceless support, care given to me from my childhood to till today and also encouraging me to achieve my goal. I would also like to thank my brother Nikhil, Durgesh and Vaibhaw, sisters Nishi, Kumkum, Amita, Preeti, Nalini and sister in law (Bhabhi) Manisha and Brother in laws (Jija) Jai Prakash Srivastava, Sanjay Prakash Srivastava, Ashit kumar Srivastava and Rajnish Kumar Srivastava for encouraging me and for their loving support all the times. I am also very much thankful to my lovely nephew Agamya Shri, Ram, Yash, Ishu, nieces Manya, Anshika and Navya for being priceless members in my life. I would also thanks to my uncles and all my relatives for their sympathy during this work.

Contents

List of Publications arising from the thesis **v**

SYNOPSIS **xviii**

List of Figures **xxv**

List of Tables **xxvii**

1 Introduction **1**

1.1 Introduction 1

1.2 The single particle shell model 4

1.3 Transfer reactions as a spectroscopic information tool 6

1.4 Motivation of the present study 7

1.4.1 Study of the reaction ^{27}Al(d,t)^{26}Al 8

1.4.2 Study of the reaction ^{27}Al(d,^{3}He)^{26}Mg 10

1.5 Outline of the present dissertation 11

2 Theoretical Formulation **13**

2.1 Reaction theory 14

2.1.1 The optical model 14

2.1.2 Distorted wave Born approximation 16

2.1.2.1 Single nucleon transfer reaction 18
2.1.2.2 Spectroscopic factors 19
2.1.2.3 Experimental spectroscopic factors 20
2.1.2.4 Method for DWBA calculation 21

3 Experimental Details and Data Analysis Technique 23

3.1 General description of facilities used in the experiment 23
3.1.1 Accelerator: Variable Energy Cyclotron 23
3.1.2 Scattering chamber 26
3.1.3 Detectors 26
3.1.3.1 Silicon detectors 27
3.1.3.2 Single sided Silicon strip detector (SSSD) 27
3.1.3.3 Double sided Silicon strip detector(DSSSD) 28
3.1.3.4 CsI(Tl) detectors 28
3.2 Description of the present experiment 30
3.2.1 Experimental setup 30
3.2.2 Electronic set-up and data acquisition 31
3.2.3 Particle identification technique 34
3.3 Offline data analysis procedure 35
3.3.1 Target thickness measurement 36
3.3.2 Gain match factor 36
3.3.3 Energy calibration of detectors 38
3.3.4 Energy loss corrections 39
3.3.5 Method to generate excitation energy 42
3.3.6 Calculation of experimental cross sections 45

4 Results and Discussions 47

4.1 Analysis of the reaction ^{27}Al(d, t) 48

4.1.1 OMP parameters for the entrance channel (d+^{27}Al). 48
4.1.2 OMP parameters for t+^{26}Al in exit channel. 50
4.1.3 DWBA Calculation for the reaction ^{27}Al(d, t) 52
4.1.4 Methodology used to extract C^2S 53
4.1.5 Results and discussions of the study of the reaction ^{27}Al(d, t) . 54
4.2 Analysis of the reaction ^{27}Al(d, ^{3}He) 62
4.2.1 OMP parameters for ^{3}He+^{26}Mg in exit channel. 62
4.2.2 DWBA calculation for the reaction ^{27}Al(d, ^{3}He) 63
4.2.3 Calculation of the C^2S values 65
4.2.4 Results and discussions of the findings of the reaction ^{27}Al(d,^{3}He). 67
4.2.5 Analog states of ^{26}Al and ^{26}Mg. 73

5 Summary and Conclusions **75**

Bibliography **81**

SYNOPSIS

Transfer reactions are very important to study the structure of nuclei. In transfer reaction, the residual nucleus may be left in any possible excited state. So, the single nucleon transfer reactions such as (d,t), (d,^{3}He) etc. give us opportunity to determine the energies of the excited states of the final product nuclei. The value of the transferred angular momentum l in a transfer reaction can be easily determined, and the spin and parity can be assigned. Apart from these important properties, spectroscopic factor for each individual excited state can be determined. So, transfer reactions open up the possibility to test the predictions of the shell model for the structure of nuclei.

In present thesis work, different excited states of ^{26}Al, populated through the reaction ^{27}Al(d,t)^{26}Al, have been studied. The nucleus ^{26}Al has recently evoked a lot of interest in nuclear physics as well as nuclear astrophysics as the decay of ^{26}Al may be used as an isotopic chronometer for galaxies; moreover it is also used to probe the Standard Model. It is well known that ^{26}Al is the first cosmic radioactivity detected through its characteristic γ rays in the interstellar medium and its lifetime ($\sim 10^6$ y) is much shorter as compared to the time for galactic evolution ($\sim 10^{10}$ y), so the detection of ^{26}Al indicates that nucleosynthesis is currently active in our galaxy and it is known that massive stars are the main sources for the origin of ^{26}Al. So it is necessary to understand the formation and destruction of ^{26}Al in our galaxy in order to understand its evolution. In addition, the observed excess of ^{26}Mg in meteorites and in presolar dust shows that the study of ^{26}Mg is also as important as ^{26}Al, because ^{26}Mg is the radioactive (β^+) decay product of ^{26}Al. So, in order to understand the formation of ^{26}Al, the study of ^{26}Mg plays a significant role.

Previously, several studies were performed using one and two nucleon transfer reactions to extract spectroscopic information about different excited states of ^{26}Al using different reaction probes. In the present thesis work, the angular distributions of various excited states of ^{26}Al produced through the reaction ^{27}Al(d,t)^{26}Al, which is the first direct study of ^{26}Al through (d,t) reaction channel, were measured. The data were then

analysed by zero-range distorted wave Born approximation calculation using the computer code DWUCK4 and spectroscopic factors for different excited states of ^{26}Al were extracted. The present study is the first direct measurement using (d,t) reaction channel to extract spectroscopic factors for different excited states of ^{26}Al. The primary motive of this measurement was to extract spectroscopic factors of different excited states of ^{26}Al using (d,t) channel and to compare the values with those obtained earlier with other reaction probes. In this work the dependence of spectroscopic factors on the potentials used as well as how much the effect of finite range parameters on spectroscopic factors were examined. Apart from several excited states of ^{26}Al, many excited states of ^{26}Mg were also observed in the present experiment. The spectroscopic factors for the different excited states of ^{26}Mg were extracted and the comparison of analog states of ^{26}Mg with the states of ^{26}Al with T=1 was made..

So, with above motivation, the experiment for this thesis work has been performed at the Variable Energy Cyclotron Centre, Kolkata, using 25 MeV deuteron beam from the K130 Cyclotron. The target was a self-supported foil of ^{27}Al (thickness~90 μg/cm^2). A three-element telescope, consisting of a single-sided 55μm thick Si(ΔE) strip detector (16 vertical strips of 3 mm width) and a double-sided 1030 μm thick Si(E) strip detector (16 strips, width 3 mm, both sides mutually orthogonal to each other) backed by four CsI(Tl) detectors (each of thickness 6 cm), was used to detect different transfer channels corresponding to various outgoing particles. The angular distributions have been measured in the angular range 16° to 40° in steps of 0.9°. Several excited states of ^{26}Al, ^{26}Mg and ^{25}Mg were produced through the reactions ^{27}Al(d, t), ^{27}Al(d, ^{3}He) and ^{27}Al(d, α). A VME-based online data acquisition system was used for collection of event - by - event data. The offline data analysis was done using ROOT based analysis programme developed in-house.

In the present thesis work two theoretical codes, ECIS94 and DWUCK4, were used for the analysis of elastic scattering and transfer channel data, respectively. The angular distribution of elastically scattered deuterons has been fitted using the optical model search code ECIS94. The parametric Wood Saxon (WS) form has been used for both

real and imaginary potentials in the optical model analysis of the elasically scaterred deuterons. Three sets of best fit optical model potential parameters were extracted and used as entrance channel potential parameters in the DWUCK4 computer code for the analysis of the angular distributions of ground as well as different excited states of ^{26}Al. Two exit channel (t + ^{26}Al) optical model parameter sets were used in DWUCK4 code. The first set of optical model potential parameters for t + ^{26}Al exit channel was obtained from the relation given by Perey and Perey and second set was taken from a previously reported ^{28}Si(d, t) work. A total of six combinations of entrance-exit channel optical model potential parameters were used to extract the spectroscopic factors for ground as well as different excited states of ^{26}Al. To extract spectroscopic factors using zero range DWBA, the following relation between the experimental and theoretical cross sections was used.

$$\left(\frac{\mathrm{d}\sigma}{\mathrm{d}\Omega}\right)_{\mathrm{exp.}} = \frac{NC^2S}{2J+1}\left(\frac{\mathrm{d}\sigma}{\mathrm{d}\Omega}\right)_{\mathrm{DWBA}}, \tag{1}$$

where, $(\frac{\mathrm{d}\sigma}{\mathrm{d}\Omega})_{\mathrm{exp.}}$ is the experimental differential cross-section and $(\frac{\mathrm{d}\sigma}{\mathrm{d}\Omega})_{\mathrm{DWBA}}$ is the cross-section predicted by the DWUCK4 code. The value of the constant N is taken from literature and it is 3.33 and 2.95 for (d,t) and (d,^{3}He) reactions respectively. J ($J = l \pm \frac{1}{2}$) is the total angular momentum of the orbital from where the nucleon is picked up. C^2 is the isospin Clebsch-Gordon coefficient and S is the spectroscopic factor.

In the present work, a detailed comparison of the present results with those obtained earlier from one neutron transfer reactions using different reaction probes was made. Actually, the relative spectroscopic factors (spectroscopic factors for different excited states of ^{26}Al relative to that of its ground state), rather than the measured values of the spectroscopic factors, were compared to take care of the uncertainty in absolute normalisation between different reaction results. The present results were also compared with the shell model calculations available in the literature for the nucleus ^{26}Al. The potential dependence of spectroscopic factors factors was also examined using two exit channel optical model potential sets mentioned above; it was found that for each exit channel with three entrance channel potential combinations the variation was

less than 10%. In the present work, spectroscopic factors were also extracted using the finite range correction value of 0.845 and nonlocal parameters of 0.54, 0.25 and 0.85 for deuteron, tritium and neutron, respectively in DWUCK4 code. Using finite range parameters, it was found that the spectroscopic factors were reduced by 20% to 50%. So, zero-range DWBA calculation was used to extract spectroscopic factors for ground as well as different excited states of ^{26}Al. The present thesis work was also motivated to study the ground as well as different excited states of ^{26}Mg produced through the reaction ^{27}Al(d, ^{3}He). Spectroscopic factors for ground as well as excited states of ^{26}Mg have been extracted and were compared with previously repoted vaues for the same. The comparison of Spectroscopic factors for analog states of ^{26}Al and ^{26}Mg have been performed.

In conclusion, the reaction ^{27}Al(d,t) was utilized for the first time to study ground and excited states of ^{26}Al. The experimental and theoretical angular distributions for both positive and negative parity states of ^{26}Al were found to be in good agreement with each other. The extracted spectroscopic factors for the observed states of ^{26}Al were found to be in good agreement with the shell model calculations available in the literature as well as with previously reported values for the same. Recently, the finding of this thesis work about spectroscopic information for ground as well as excited states of ^{26}Al upto an excitation of 5.50 MeV using zero range DWBA calculation has been published in Physical Review C and some of the data were presented at the FUSION14 conference. Some of the data of ^{26}Al was also presented DAE symposium on Nuclear Physics 2014 in BHU, Varanasi, India and also in Nucleus-Nucleus Collisions 2015 conference in Catania, Italy(oral presentation). The reaction ^{27}Al(d, ^{3}He) was also studied to extract spectroscopic information of the ground as well as excited states of ^{26}Mg. The observed analog states of ^{26}Al and ^{26}Mg for T=1 were also studied. The data of ^{27}Al(d, ^{3}He) will be submitted for publication very soon.

Signature of the student: Vishal Srivastava

Date: 10-08-2015

The synopsis for the thesis is approved by the doctoral committee.

Mentoring / Doctoral Committee

S. No.	Name	Designation	Signature	Date
1.	Dr. S. R. Banerjee	Chairman		10/8/2015
2.	Dr. C. Bhattacharya .	Convener	C. Bhattacharya	10/8/2015
3.	Dr. Subinit Roy	Member	Subinit Roy	10/8/15
4.	Dr. G. Mukherjee	Member		10/08/2015

List of Figures

1.1 Single particle nuclear levels according to shell model. 5

3.1 K130 Variable energy cyclotron with switching magnet and various beam lines. 24

3.2 Layout of different beam lines of K130-cyclotron. 26

3.3 (a)Single sided Si(ΔE) and double sided Si(E) strip detectors and (b) Four CsI(Tl) detector placed on each other. 29

3.4 A schematic sequence and view of different elements telescope. . . . 29

3.5 Detector telescope setup used in the present experiment. 31

3.6 (a)Typical two dimensional spectra obtained using Si(ΔE) strip Vs. Si(E) strip detector telescope and (b) obtained using Si(E) strip Vs. CsI(Tl) detector telescope. 32

3.7 The electronic setup used in the present experiment. 33

3.8 Schematic block-diagram of the electronic setup. 33

3.9 Two dimensional spectra obtained using pulser for the 3^{rd} and 12^{th} strips of Si(ΔE) strip Vs. Si(E) strip detector telescope. 38

3.10 Typical two dimensional spectrum obtained after gain matching at $\approx 36^0$. 39

3.11 (a) Projection of ^{3}H ridge and (b) Prejection of ^{3}He ridge onto the (E + ΔE) axis at $\approx 36^0$. 40

3.12 (a) Energy calibration of 3^{rd} and 14^{th} strips of Si(E) strip detector using seven known states of ^{26}Al while (b) represents the enaergy caliberation using three states of ^{26}Mg and ground state of ^{26}Al. 41

3.13 Excitation energy spectra of ^{26}Al obtained at $\theta_{lab} \approx 28^{\circ}$ (solid line) and at $\theta_{lab} \approx 38^{\circ}$ (dash-dash). Excitation energies labeled inside the figure are in keV. 43

3.14 Excitation energy spectra of ^{26}Mg obtained at $\theta_{lab} \approx 18^{\circ}$ (dash line) and at $\theta_{lab} \approx 36^{\circ}$ (solid line). Excitation energies labeled inside the figure are in keV. 44

4.1 Angular distributions of elastically scattered deuteron from ^{27}Al at E_{lab} = 25 MeV (present data) and 23 MeV. The filled circles represent experimental data, solid and dash-dash lines represent optical model fits for set A and set B, respectively. 49

4.2 Comparison of experimental and theoretical angular distributions for the ground, 230, 1056, 1762 and 1848 keV states. Filled circles are the present experimental data. Solid and dash-dash lines are theoretical predictions from DWUCK4 code for pick up from $0d_{5/2}$ with set A-A1 and set A-B1, respectively. 55

4.3 Same notations as in Fig. 4.2 for the 420 keV state . The upper plot (a), represents calculation for pick up from $1s_{1/2}$ and lower plot (b), represents calculation for pick up from $0d_{5/2}$. 56

4.4 Same notations as in Fig. 4.2 for the 2070, 2367, 2542, 3160 and 3409 keV states for pick up from $0d_{5/2}$. 59

4.5 Same notations as in Fig. 4.2 for the 3505 keV state for pick up from $0g_{9/2}$. 60

4.6 Same notations as in Fig. 4.2 for the 4443 keV state for pick-up from $0p_{1/2}$. 60

4.7 Same notations as in Fig. 4.2 for the 4719 keV state for pick up from $0d_{5/2}$. 60

4.8 Same notations as in Fig. 4.2 for the ground and 1056 keV states but theoretical predictions from DWUCK4 code for pick up from $0d_{5/2}$ includes finite range and non local corrections. 62

4.9 Angular distributions for ground, 1806, 2935 and 4335 keV states.The filled circles represent experimental data points and solid line represents theoretical cross section from DWUCK4 code for the OMP combination A-B for considering pick up from $0d_{5/2}$ only, dash-dot-dash represents theoretical cross section for A-B with pick up from $1s_{1/2}$ only while dash-dash represents the theoretical cross sections for $0d_{5/2}$ + $1s_{1/2}$ mixing. Note that theoretical cross sections were normalized to experimental data points. 68

4.10 Angular distributions for 4847, 5302, 5482, 5718 and 6141 keV states (same notations as in Fig.4.9). 69

List of Tables

3.1 Technical specifications of K130 cyclotron. 25

4.1 The best fit potential parameters used in DWUCK4 code for ^{27}Al(d,t) reaction. 51

4.2 Extracted C^2S values for different states of ^{26}Al for the reaction ^{27}Al(d,t). 52

4.3 Comparison of C^2S/C^2S_{gs} of the present study with those obtained from other experimental studies done using different reaction probes for different states of ^{26}Al. 57

4.4 The best fit potential parameters used in DWUCK4 code for ^{27}Al(d,^{3}He) reaction. 64

4.5 Extracted values of C^2S for different excited states of ^{26}Mg from the reaction ^{27}Al(d,^{3}He) at 25 MeV. 70

4.6 Comparison of C^2S/C^2S_{gs} of the present study with those obtained from other experimental studies done using same reaction probe at different energies for different states of ^{26}Mg. 71

4.7 Comparison of spectroscopic factor S of T=1 analog states observed in the reactions ^{27}Al(d,t)^{26}Al and ^{27}Al(d,^{3}He)^{26}Mg at 25 MeV. 73

Chapter 1

Introduction

1.1 Introduction

We know that the basic constituents of matter are atoms which are composed of electrons and a core nucleus. Several attempts have been made to understand the structure of the atom. In 1911, Rutherford's experiment gave some idea about the composition of atom and Bohr's atomic model suggested the existence of discrete electronic orbits around the positive nucleus. The successive attempts to know about the composition of nucleus led to the discovery of neutron by J. Chadwick in 1932. After the discovery of neutrons it was concluded that the nucleus is composed of protons and neutrons. Further development in science and technology leading to the building of powerful accelerators helped probing the nucleus with energetic projectiles to understand the structure of different nuclei. With the availability of high energy beam at present, we are able to probe the substructure of nucleons and know about the smallest constituents of matter called quarks. Broadly, the experimental nuclear physics is categorised as low energy and high energy nuclear physics depending upon the incident energy. In low energy experimental nuclear physics, most of the experiments are performed to probe the properties of nucleus (usually upto several tens of MeV energy) and the nuclear structure related informations are extracted. On the other hand, the

aim of the high energy nuclear physics experiment (1Gev/nucleon and above) is to probe the subatomic degrees of the freedom in general. In between these two energy domains, there are intermediate energies (typically 0.1-1Gev/nucleon) where one can extract information on properties of nuclear matter as well as mechanism of production of various particles like pions, kaons etc.

The light and heavy ion induced low energy nuclear reactions are the powerful tools to probe the structure of nuclei. These reactions can be broadly divided into two types as direct nuclear reactions and compound nuclear reactions. On the basis of interaction time between the two colliding nuclei, these processes are categorised. At low energies(<< 10 MeV/nucleon, close to coulomb barrier), the incident particle either scatters elastically without loss of appreciable energy or fuse with target to form a compound nucleus. As the incident energy is increased, other reaction mechanism like direct reactions, becomes significant. The typical time of interaction for direct nuclear reaction is $\approx 10^{-22}$ seconds. In this short interaction time, only a few particle exchange may take place between the colliding nuclei; The target nucleus as a whole is not disturbed but for particle transfer to mostly bound single particle states- leading to single particle excitation of the recoiling nucleus. On the other hand, typical interaction time for compound nuclear reaction is $\approx 10^{-16}$ seconds. In compond nuclear reaction, available energy is redistributed among the colliding nucleons leading to the formation of highly excited compund nucleus. These processes can be expressed in terms of equation using the projectile (a), target (A), ejectile (b) and recoil nucleus (B) using following relations;

Reaction	Type
$a + A \longrightarrow b(x + a) + B(A - x)$	Pickup
$a + A \longrightarrow b(a - x) + B(A + x)$	Stripping
$a + A \longrightarrow x + a + B$	Knockout
$a + A \longrightarrow C^{*}$	Compound Nuclear

The first two (pickup and stripping) reactions come under the transfer reaction; they are important as we can produce the nuclei of interest using suitable target projectile combinations and can also extract spectroscopic information about the structure of nuclei. Every nuclear reaction follows some conservation laws like energy, linear and angular momentum conservation etc. The details about the nuclear reaction dynamics and conservations laws are given in [Sit01, Gsh01, Ren01, Ber01]. In direct nuclear reactions the transition probabilities from the entrance to exit channel is estimated using the initial and final state wave functions to compute the nuclear transition matrix. The overlap wave functions are estimated in direct reaction theory to extract spectroscopic information of the nuclei of interest produced through particular transfer reaction. The direct reaction theory was first developed using plane wave Born approximation(PWBA) where both initial and final states are represented by plane waves. The angular distributions predicted from PWBA theory were found to reproduce only first or upto second peaks in the experimental cross section. As the experimental cross sections contain the coulomb as well as the nuclear effects, the wave functions should also carry their signatures; therefore PWBA may not be a good approximation. Later, the shortcomings of the PWBA were removed using distorted waves as the initial and final wave functions instead of plane waves and the new technique was termed as distorted wave Born approximation (DWBA). In DWBA theory, elastic scattering is taken as the main process to occur while transition to other reaction channels are taken as small perturbation. The distorted waves are generated from the optical model potential(OMP) which are extracted by fitting the angular distribution of elastic scattering cross sections for both entrance and exit channels separately. Relevant descriptions of the OMP and DWBA are given in chapter 2. The direct reaction theory has been developed for both single and multinucleon transfer reactions. The details of direct reaction theory and its application are available in [Sat01, Sat02, Sit01, Ren01]. The structural informations extracted from experiments need comparison with suitable theoretical predictions and vice-versa to confirm the validation of the observations and predictions.

1.2 The single particle shell model

Several theoretical models like shell model and collective model have been developed to understand the structure of nuclei. The shell model, which is mainly a single particle model, was very successful in describing the single particle structure of nucleus. The basic assumption of the shell model is that each nucleon experiences an average interaction potential created by all nucleons of the nucleus. Unlike the atomic case, no central agency is known to exist in the nucleus. However, it was assumed that the nucleons are moving independently in an average central potential; so it is possible to obtain the solution of the Schroedinger wave equation for the motion of an individual nucleon in this field. The nuclear hamiltonian for shell model can be written as;

$$H = H^0 + H_{res} \tag{1.1}$$

Where, $H^0 = \sum_{i=1}^{A} h_i$ is the Hamiltonian for the indepedent particles in average potential and H_{res} represents the hamiltonian for residual interaction. The sequence of the single particle nuclear levels according to the shell model is shown in Fig. 1.1.

In shell model, individual levels are described in terms of quantum numbers (n,ℓ,j) as shown in Fig. 1.1. As in case of atomic physics, the degeneracy of each level, which is the number of nucleons that can be accommodated in each level, is $2(2\ell + 1)$. The factor $(2\ell + 1)$ arises from the m_ℓ (projection of angular momentum, ℓ) degeneracy and the additional factor 2 comes from the m_s (projection of spin, s) degeneracy. At the initial stage, spin-orbit interaction was not included in the average potentials but later Mayer, Haxel, Suess and Jensen introduced spin-orbit potential in the average mean field potential. By the inclusion of the spin-orbit interaction, observed shell closures (and corresponding magic numbers) are successively reproduced. The residual interaction between the loose nucleons in the outermost level does not cause any perturbation of the single particle levels determined by (n, ℓ, j). It is usually assumed that the residual interaction is weak compared to the spin-orbit interaction so that the

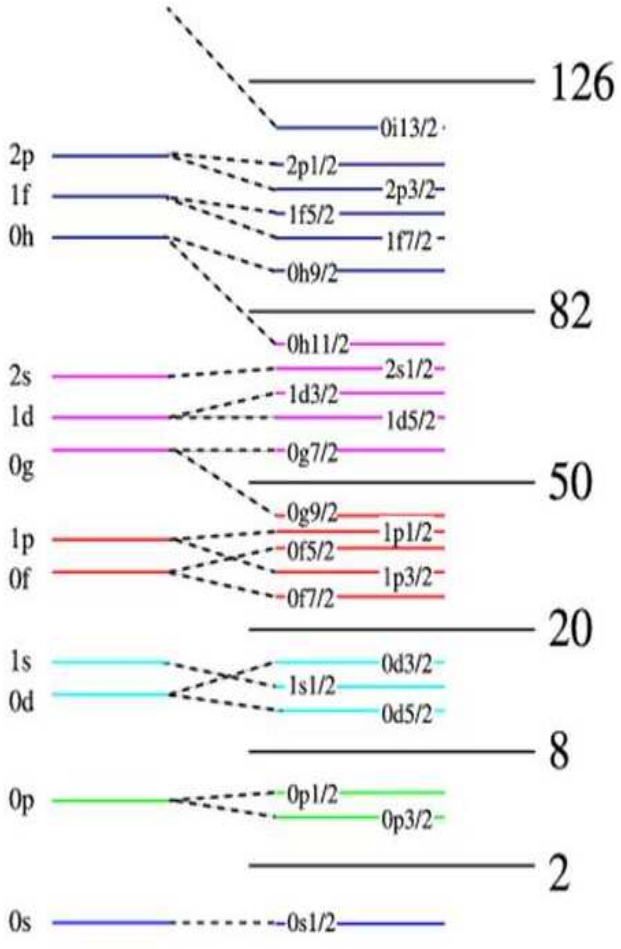

Figure 1.1: Single particle nuclear levels according to shell model.

j still remains a good quantum number and levels will characterized by definite j values. If this is not the case, then the particles may be regarded as the superposition of different (n, ℓ, j) states with energies close to one another. This is known as configuration mixing. The details of the shell model and their application can be found in [Pal01, Hyd01, Gsh01, Kra01, Pbh01].

1.3 Transfer reactions as a spectroscopic information tool

The types of transfer reactions given in 1.1 provide us opportunity to determine the excitation energy, spin, parity, orbital and total angular momentum and also the spectroscopic factors for single particle levels of the nuclei of interest. The main feature of the transfer reactions is that the recoil nucleus may be left in any of the excited states. The experimentally extracted angular distributions can be directly compared with those predicted theoretically using different transfer reaction codes and we can easily extract the spectroscopic factors for different populated excited states of the recoil nucleus. Spectroscopic factor measures the degree to which a state populated in a transfer reaction is a single-particle state [Gle01]. Spectroscopic factor describes the single particle orbital structure of the observed state. Basically, spectroscopic factors give us the information about the occupancy of the single particle orbital. If Φ_A and Φ_B are the intial and final wave functions of the nuclei A and B before and after the reaction, the norm of the overlap function $I_{BA} = \langle \Phi_A \mid \Phi_B \rangle$ gives the spectroscopic factor(SF).

The differential cross section for the reaction a + A $\longrightarrow$ b + B is proportional to the square of the transition amplitude and can be written as;

$$\frac{d\sigma}{d\Omega} \propto \sum_{l j m_l} \mid S_{\ell j} B_{\ell}^{m_\ell} \mid^2. \tag{1.2}$$

Where, $S_{\ell j}$ is the spectroscopic factor and $|B_{\ell}^{m_\ell}|^2$ contains all of the kinematic dependence through the wave functions of the relative motion and their overlap with each other. In addition, it contains the nuclear wave function of the transferred particle. $|B_{\ell}^{m_\ell}|^2$ has angular dependence that depends on ℓ and the value of ℓ can be determined by a comparison with experiment. If the initial states are known then using total angular momentum ($J = \ell + s$) conservation and parity selection rules $(-1)^{\ell}$ between the intial and final states, we can determine the final states. The theoretical cross sections calculated are compared with the experimental cross sections to extract the experimental spectroscopic factors [Gle01].

Experimental spectroscopic factor is defined as the ratio of experimental cross sections to the theoretically predicted cross sections. Maintaining total angular momentum conservation, theoretical cross sections are calculated for different ℓ-values and the ℓ-value for which the shapes of the theoretical and experimental angular distributions match is taken to be the value of required single particle orbital. Theoretically predicted cross sections are obtained using distorted wave Born approximation(DWBA) code DWUCK4 [kunz01]. The details of the DWBA theory and DWBA calculations can be found in [Sat01, Sat02, Sat03, Gle01]. The DWBA theory takes into account both the scattering and loss of flux (absorption) of particle. Experimentally extracted spectroscopic factors can be directly compared with those predicted theoretically using different nuclear models like shell model etc. and we can test the predictions from the shell model for the single particle structure of nuclei.

1.4 Motivation of the present study

Since spectroscopic factor gives the structure related information of nuclei, so it should be independent of reactions involved as well as energies. But, it was observed that it does not always remain constant and may differ for different reaction probes used to study the nuclei. Distorted wave Born approximation method (DWBA) is used to

calculate the theoretically predicted cross sections and distorted waves are generated by the optical model potential parameters separately for entrance and exit channels, So, the normalization between theoretical cross sections and experimental cross sections may differ for different reactions probes. From this short discussion one may conclude that due to the choice of optical potentials, spectroscopic factors may come out to be different [Lee01, Lee02, End05, Tsa01]. So, first point is that the examination of extracted spectroscopic factors for particular nucleus using different reaction probe and its comparison using other reaction probes is necessary. Secondly, if one extracts spectroscopic factors for a particular nucleus of interest using same reaction probe but using different optical model potentials, then also the comparison is necessary to examine the consistency of the spectroscopic factors.

1.4.1 Study of the reaction ^{27}Al(d,t)^{26}Al

In the present thesis work, one neutron and one proton pick up reactions on ^{27}Al target have been studied. The main aim of the present thesis work is to extract spectroscopic factors for the different observed states of ^{26}Al and ^{26}Mg populated through the ^{27}(d,t)^{26}Al and ^{27}Al(d,^{3}He)^{26}Mg reactions. The reason for choosing the reaction ^{27}Al(d,t)^{26}Al is that the nucleus ^{26}Al has recently created a lot of interest as it is the first cosmic radioactivity detected through its characteristic gamma rays in the interstellar medium. Since its lifetime ($\sim 10^{6}$ y) is much shorter as compared to the time for galactic evolution ($\sim 10^{10}$ y), the detection of ^{26}Al at the present time indicates that nucleosynthesis is currently active in our galaxy and it is known that massive stars are the main sources for the origin of ^{26}Al [Dieh01, Pran01]. There are also evidences that short-lived nuclei were present in the early solar system [Wass01] and it is, therefore, necessary to understand the formation and destruction of ^{26}Al in our galaxy in order to understand its evolution. So, from astrophysics as well as basic nuclear physics points of view, the nucleus ^{26}Al has evoked lot of interest - as the decay of ^{26}Al may be used as an isotopic chronometer for galaxies [Fit01]; moreover it is also used to probe the

Standard Model [Fin01, Sat04]. However, the astrophysical interest of ^{26}Al is beyond the scope of the present thesis work. The spectroscopic factors of the observed states of ^{26}Al populated through the ^{27}Al(d,t) reaction are the main focus of this work which is the first direct study of ^{26}Al using (d,t) reaction channel.

In previous years many of the states of ^{26}Al have been studied using different reaction channels, like ^{28}Si(p,^{3}He) [Chip01], ^{28}Si(d,α) and ^{24}Mg(^{3}He,p) [Tak01], ^{27}Al(p,d) [Kro01, Shw01], ^{27}Al(^{3}He, α) [Bet01, Nur01]. In addition, an attempt has been made in the past to study the ^{27}Al(d,t) reaction up to 2.08 MeV excitation energy using off-line measurements of captured tritium activity in stacked ^{27}Al foils [Vla01]; however, no direct measurement of the ^{27}Al(d,t) reaction has so far been available, to the best of our knowledge, in the literature. The spins, parities and branching ratios for different excited states of ^{26}Al have been compiled by Endt [End01] and studied by Endt *et al*. [End02, End03]. Attempts have also been made to understand the structures of the excited states of ^{26}Al theoretically in terms of the shell model; comparison of spectroscopic factors up to 4.699 MeV have been made with a $0d_{5/2}$-$1s_{1/2}$ shell model scheme [Kro01]. Furthermore, from the calculation of spectroscopic factors for several excited states of ^{26}Al, it was shown that C^2S values for the low-lying states are in good agreement with shell-model predictions [Bet01]. Relative spectroscopic factors for several excited states of ^{26}Al have also been extracted and compared [Shw01, Nur01].

In the present thesis work, the reaction ^{27}Al(d,t)^{26}Al has been studied at 25 MeV beam energy with the motivation to extract spectroscopic factors of the ground as well as different excited states populated in the reaction. The spectroscopic factors for fourteen excited states of ^{26}Al have been extracted using zero-range distorted wave Born-approximation (DWBA) calculations and compared with earlier reported values obtained using other single neutron pick up reactions. Relative spectroscopic factors (calculated using the value of the ground state spectroscopic factor to be one) extracted from the present data have also been compared with those reported earlier for other pick-up reactions. Shell-model results have been taken from [Kro01] and [Bet01] to compare with the present results.

1.4.2 Study of the reaction ^{27}Al(d,^{3}He)^{26}Mg

In a similar way, the nucleus ^{26}Mg is also important from nuclear physics as well as nuclear astrophysics points of view as it is the radioactive decay product of ^{26}Al. Very recent study of the reaction ^{23}Na(α,p)^{26}Mg indicated that the reaction ^{23}Na(α,p)^{26}Mg directly influences the production of ^{26}Al [Alm01]. Being the radioactive decay product of ^{26}Al, the observed excess of ^{26}Mg in meteorites [Phe01], presolar dust [Hop01, Hus01] and the presence of excess ^{26}Mg resulting from the decay of ^{26}Al in calcium-aluminium-rich inclusions (CAIs) and ferromagnesian silicate spherules (chondrules) from Allende meteorite [Biz01] shows that the study of ^{26}Mg is also important to understand the origin of ^{26}Al.The spectroscopic factors of T=1 analog states of ^{26}Al and ^{26}Mg should be identical, so the verification of T=1 analog states in ^{26}Al and ^{26}Mg produced in (d, t/ ^{3}He) reaction sequence was also the motivation of the present study, which is the first study using ^{27}Al(d, t) and ^{27}Al(d,^{3}He) reactions sequence.

In previous years, several particle transfer reactions were performed to study the different excited states of ^{26}Mg. Earlier, reaction (d,^{3}He) has been studied at 29 MeV [Ver01], 34.5 MeV [Wil01], 52 MeV [Wag01] and at 80 MeV [Ard01]. Apart from (d,^{3}He) reaction channel, other reaction channels such as ^{25}Mg(α,^{3}He) [JKra01, Yas03] and ^{25}Mg(d,p) [Burl01] were also used to study ^{26}Mg. The spectroscopic factors for the excited states of ^{26}Mg have been extracted in these reactions. A compilation of different excited states of ^{26}Mg has been performed by Endt *et al*. [End01, End04].

In the present thesis work, nine excited states of ^{26}Mg were studied by zero range distorted wave Born approximation calculations and the extracted values of spectroscopic factors were compared with the previous results using same reaction probe and also with predictions from the shell model given in [Wil01, Wag01] and predictions given from rotational model in [Wag01]. In previous years, in Refs. [Bet01, Yas03, Wag01], the analog isobaric states of ^{26}Al and ^{26}Mg were also compared but the comparison of T=1 analog isobaric states using ^{27}Al(d, t) and

^{27}Al(d,^{3}He) reactions sequence was not performed ever before. In this thesis work, the T=1 analog states observed in the present study of both the reactions ^{27}Al(d,t)^{26}Al and ^{27}Al(d,^{3}He)^{26}Mg were also compared by their corresponding spectroscopic factors.

1.5 Outline of the present dissertation

This thesis work is arranged in five chapters in the following manner. Chapter 2 contains all the theoretical formulations used in the present work. Chapter 2 begins with the introduction of optical model potential followed by the brief description of DWBA theory. A short introduction of spectroscopic factor is presented which is followed by the method to extract the theoretically predicted cross sections from the DWUCK4 code. The chapter 2 ends with a brief discussion on the calculation of experimental spectroscopic factors. The details of the experiment performed for the present thesis work and data analysis proceedure are given in chapter 3. After these chapters, chapter 4 contains the detailed results and discussions of the study of the reactions ^{27}Al(d,t)^{26}Al and ^{27}Al(d,^{3}He)^{26}Mg. Finally, the summary and conclusions are given in chapter 5.

Chapter 2

Theoretical Formulation

This chapter contains brief descriptions of various theoretical reaction formalisms and the related computer codes used in the analysis of experimental data. The present study deals with one neutron and one proton pick up reactions ^{27}Al(d,t)^{26}Al and ^{27}Al(d,^{3}He)^{26}Mg with the motivation to extract the spectroscopic factors for ground as well as different excited states of ^{26}Al and ^{26}Mg. The zero range distorted wave Born approximation (ZR-DWBA) calculation was performed to extract the spectroscopic information. Before performing ZR-DWBA calculation, we have extracted optical model potential parameters to describe the elastic scattering of deutron from ^{27}Al target and have also searched for suitable sets of optical model potential parameters for tritium and helium-3 in the exit channels separately. After getting the best optical model parameters, we performed the calculation of ZR-DWBA. So, in this chapter we have started with the brief discussion of optical model followed by the discussion on the basics of distorted wave theory. Finally, a short introduction and the procedure for extraction of spectroscopic factors have been discussed.

2.1 Reaction theory

2.1.1 The optical model

The effect of any nuclear collision (other than the elastic scattering) is to remove the system from the entrance channel, by way of either inelastic scattering or nuclear reactions - which is generally termed as 'absorption'. This usually happens when the colliding nuclei are quite close to each other. Earlier, it is assumed that upto some nuclear radius $r \approx R$, there is strong absorption and compound nucleus formation while the plane wave form is retained for $r \geq R$. A more realistic way to explain the general features of nuclear reaction is to introduce a complex potential model called 'The Optical Model Potential(OMP)'. The establishment of the basis of the optical model was given in [Herm01]. The real part of the OMP represents the nuclear interaction between target and projectile and also describes the elastic scattering while imaginary part of the OMP is responsibile for the absorption or the loss of flux from the elastic channel. The complex OMP can be written as follows,

$$U(r) = U_R(r) + U_I(r) + U_D(r) + U_{SO}(r) + U_C(r) \tag{2.1}$$

or in complete parametric form as,

$$U(r) = -Vf(r, R, a) - iWf(r, R_I, a_I) + 4ia_I W_D \frac{df(r, R_I, a_I)}{dr}$$

$$+ \vec{s}\,.\,\vec{\ell}\, V_s \frac{1}{r}\frac{df(r, R_s, a_s)}{dr} + U_C(r) \tag{2.2}$$

where, (R, a), (R_I, a_I) and (R_s, a_s) represent radius and diffuseness parameters for the real, imaginary, and spin-orbit potentials, respectively. The parameters of the OMP depend upon the energy and the mass of the reactants (mass of target and projectile), So the parameters are adjusted to reproduce the elastic scattering data accurately. The parametric Wood-Saxon form is used for both real and imaginary part of the potential parameters to fit the experimental data. The Wood-Saxon form factor f(r,R, a) has the

following form,

$$f(r, R, a) = \frac{1}{1 + e^{\frac{r-R}{a}}} \tag{2.3}$$

The $U_I(r)$ and $U_D(r)$ parts of the OMP are responsible for the absorption of flux or particles in nuclear reactions from elastic channel. The $U_I(r)$ is the volume imaginary part and it is responsible for the absorption in the whole volume of the nucleus while the $U_D(r)$ acts specifically in the region close to the nuclear surface because of the derivative of function f. At high energy, the volume imaginary part plays the significant role while at low energies, the surface part becomes more significant. The fourth term of Eqn. 2.2 is the spin orbit interaction term and it is also important on the surface of the nucleus because it also contains derivative of function f. This potential is necessary to check the polarisation effect in experimental value. Finally, the last term in Eqn. 2.2 is the Coulomb interaction term and it has the form;

$$U_C(r) = \frac{Z_1 Z_2 e^2}{2R_c}\left(3 - \frac{r^2}{R_c^2}\right) \qquad (r \leq R_c) \tag{2.4}$$

$$= \frac{Z_1 Z_2 e^2}{r} \qquad (r > R_c) \tag{2.5}$$

Where, R_c, is the coulomb barrier radius with other symbols have their usual meanings.

In the present work, the optical model search code ECIS94 [Ran01] was used to extract the optical model potential parameters for the entrance channel d+^{27}Al. The parameters of the phenomenological OMP are adjusted to reproduce the correct experimental data by minimization of χ^2. After best fit, we get the required optical model potential parameters and these will be used for the analysis of the transfer reaction data to extract the spectroscopic information. Two sets of OMP parameters, one each for t+^{26}Al and ^{3}He+^{26}Mg in the exit channels were obtained from the relation given in [Per01]. The detailed procedure of extraction of OMP parameters is given in analysis and discussion in chapter 4.

2.1.2 Distorted wave Born approximation

To understand the distorted wave Born approximation, let us start with the simple plane wave form for both entrance and exit channel wave functions. Let us start with the process A(a,b)B to understand the DWBA formalism. The transition amplitude for this reaction within Born Approximation may be written as

$$T_{BA} = \int e^{-i\vec{k}_b.\vec{r}_b} \langle \Psi_B \Psi_b \mid V \mid \Psi_A \Psi_a \rangle e^{i\vec{k}_a.\vec{r}_a} d\vec{r}_a d\vec{r}_b \tag{2.6}$$

Where, $\vec{k}_a$ is the relative momentum and $\vec{r}_a$ the separation of the centre of mass of nuclei a and A, while $\vec{k}_b$, $\vec{r}_b$ are the corresponding quantities in the exit channel b + B. The quantity Ψ_i represents the internal state of the i^{th} nucleus (a, A, b and B). V is the interaction potential that causes the ”transition” from the entrance to the exit channel. In this section the physics description and notations follow the direct reaction theory given in [Sat02]. Assuming that nuclear forces (embodied in V) are of short range, we may approximate $\vec{r} \approx \vec{r}_b \approx \vec{r}_a$ (which means that ’b’ is emitted from the same point at which ’a’ is absorbed). This leads to,

$$T_{BA} \cong \int e^{i\vec{Q}.\vec{r}} \langle \Psi_B \Psi_b \mid V \mid \Psi_A \Psi_a \rangle d\vec{r} \tag{2.7}$$

where $\vec{Q} = \vec{k}_a - \vec{k}_b$ is the momentum transfer. The matrix element $\langle \Psi_B \Psi_b \mid V \mid \Psi_A \Psi_a \rangle$ represents an integration over the internal coordinates. We may write it as a multipole series as,

$$\langle \Psi_B \Psi_b \mid V \mid \Psi_A \Psi_a \rangle = \sum_{\ell,m} f_\ell(r) Y_\ell^m(\theta, \phi). \tag{2.8}$$

The nuclear spins, and possibly structural selection rules, result in only one or few values of ℓ (this ℓ is same as the ‘ℓ’ of the orbit from where the particle is removed). If we consider only one term and select the corresponding ℓ^{th} partial wave from $e^{i\vec{Q}.\vec{r}}$; then the equation 2.7 reduces to

$$T_{BA} \propto \int j_\ell(Qr) f_\ell(r) r^2 dr \tag{2.9}$$

If we assume that the reaction is confined to the nuclear surface $r \approx R$, then we get the characteristic dependence of the transition amplitude on the multipolarity or the

angular momentum transfer l as follows:

$$T_{BA} \propto j_{\ell}(Qr) \tag{2.10}$$

where ,

$$Q = [k_a^2 + k_b^2 - 2k_a k_b \cos(\theta)]^{1/2} \tag{2.11}$$

and θ is the direction of emission of b relative to the incident beam. Here $\vec{Q}$ is the momentum transfer and it is a consequence of momentum conservation. From the angular momentum conservation, we can determine the value of ℓ. The plane wave Born approximation (PWBA) predicts accurately the first peak in the angular distribution but fails to predict total angular distribution accurately. The magnitude of the cross sections predicted in PWBA were in disagreement with the measured ones. Since in the measured angular distributions, the coulomb as well as nuclear potentials play significant role: the PWBA approximation can not explain the total angular distributions accurately because the plane wave has been distorted due to the presence of the said two potentials. The main drawback comes from the concept of surface reaction. The nuclear interior r < R has been excluded by assuming that at some nuclear radius r = R there is strong absorption due to compound nucleus formation while the plane wave form has been retained for r ≥ R. So, to correct the PWBA for incoming and outgoing particles, the concept of distorted wave Born approximation has been introduced to account for the nuclear interior. So, instead of plane waves, if we use distorted waves that contain the plane wave and the part dispersed elastically by the presence of optical potential, then the Born approximation is called distorted wave Born approximation. The distorted wave $\chi^{(\pm)}(\vec{k}, \vec{r})$ asymptotically describe a plane wave with momentum $\vec{k}$ plus an outgoing (or incoming) spherical scattered wave which in the case of no coulomb potential has the form,

$$\chi^{(\pm)}(\vec{k}, \vec{r}) \longrightarrow e^{i\vec{k}.\vec{r}} + f(\theta)\frac{e^{\pm i\vec{k}.\vec{r}}}{r} \tag{2.12}$$

Where χ^{+} and χ^{-} represent the distorted wave in the entrance and exit channel respectively and $f(\theta)$ represents the scattering amplitude [kunz01]. The transition amplitude

in DWBA for the reaction A(a,b)B can be written as,

$$T_{DWBA} = \int \chi^{(-)}(\vec{k}_b, \vec{r}_b)^* \langle \Psi_B \Psi_b \mid V \mid \Psi_A \Psi_a \rangle \chi^{(+)}(\vec{k}_a, \vec{r}_a) d\vec{r}_a d\vec{r}_b \tag{2.13}$$

The χ's are generated by using optical potentials whose parameters have been adjusted to fit the observed elastic scattering at appropriate energy.

2.1.2.1 Single nucleon transfer reaction

The DWBA theory assumes that the elastic scattering is the most important process to occur when two nuclei collide and the removal of flux into many other reaction channels is considered as pertubations. If α, β denote the entrance and exit channels respectively. Then the transition amplitude for the process A(a,b)B can be written as,

$$T_{\beta\alpha} = \int \chi^{(-)}(\vec{k}_\beta, \vec{r}_\beta)^* \langle \Psi_\beta \mid V \mid \Psi_\alpha \rangle \chi^{(+)}(\vec{k}_\alpha, \vec{r}_\alpha) d\vec{r}_\alpha d\vec{r}_\beta \tag{2.14}$$

Where,

$$\langle \Psi_\beta \mid V \mid \Psi_\alpha \rangle = \langle \Psi_B \Psi_b \mid V \mid \Psi_A \Psi_a \rangle$$

Where, the relative momenta of a and b are $\hbar k_\alpha$ and $\hbar k_\beta$ respectively, and χ's in terms of α and β represents the relative motion of the particle **a** towards A and b towards B respectively. The relation between differential cross section and transition amplitude is given by,

$$\frac{d\sigma}{d\Omega} \propto \mid T_{\beta\alpha} \mid^2 \tag{2.15}$$

Since in the present work, the structure of ^{26}Al and ^{26}Mg have been investigated using the single nucleon transfer reactions ^{27}Al(d,t) and ^{27}Al(d,^{3}He). The equation 2.14 for the reactions ^{27}Al(d,t)^{26}Al and ^{27}Al(d,^{3}He)^{26}Mg can be written as,

$$T_{(d,t)} = \int \chi^{(-)}(\vec{k}_t, \vec{r}_t)^* \langle \Psi_\beta \mid V \mid \Psi_\alpha \rangle \chi^{(+)}(\vec{k}_d, \vec{r}_d) d\vec{r}_d d\vec{r}_t \tag{2.16}$$

and

$$T_{(d,^3He)} = \int \chi^{(-)}(\vec{k}_{^3He}, \vec{r}_{^3He})^* \langle \Psi_\beta \mid V \mid \Psi_\alpha \rangle \chi^{(+)}(\vec{k}_d, \vec{r}_d) d\vec{r}_d d\vec{r}_{^3He} \tag{2.17}$$

respectively.

2.1.2.2 Spectroscopic factors

The factor $\langle \Psi_\beta \mid V \mid \Psi_\alpha \rangle = \langle \Psi_B \Psi_b \mid V \mid \Psi_A \Psi_a \rangle$ of eqn. 2.14 is called the 'form factor' or the 'transfer function'. This is a function of r_α and r_β. This factor plays the role of an effective interaction for the transition from the elastic scattering state $\chi^{(+)}$ to $\chi^{(+)}$ and contains all the nuclear structure related informations. Basically it includes two nuclear overlaps: (a) $\langle \Psi_B \mid \Psi_A \rangle$ called target form factor and (b) $\langle \Psi_b \mid \Psi_a \rangle$ called projectile form factor. The measurement of overlap of this kind is the spectroscopic factor [Sat02]. A brief introduction of such measurements is as follows; we can define the meaurements of the said two types of nuclear overlaps for the reaction type $a(= x + b) + A \longrightarrow b + B(= A + x)$ as follows; $S_{\ell_1, j_1}(b, x \mid a)$ for the system 'a' that gives the probability that when it is in the state Ψ_a, it will be found to be composed of the entity 'x' with orbilal angular momentum ℓ_1 and total j_1 relative to the product nucleus 'b' in the state Ψ_b and similarly $S_{\ell_2, j_2}(A, x \mid B)$ for the system 'B' that gives the probability that when it is in the state Ψ_B, it will be found to be composed of the entity 'x' with orbilal angular momentum ℓ_2 and total j_2 relative to the product nucleus 'A' in the state Ψ_A. Pick-up reaction is the inverse of the stripping reaction. Pickup reaction $a + A(= x + B) \longrightarrow b(= x + a) + B(= A - x)$, populates states in the nucleus A that are built on the ground state of B [Sat02]. Measurements of these types give us the spectroscopic factors. The main importance of the spectroscopic factor is that it represents the degree to which a state populated in a transfer reaction is a single-particle state and it provides us the opportunity to test the predictions from shell model regarding the sigle particle state of the nuclei of interest [Gle01].

In the present thesis work, zero range distorted wave Born approximation (DWBA) calculation was performed to extract spectroscopic informations about the single particle orbitals of ^{26}Al and ^{26}Mg. In zero range DWBA calculation, the projectile form factor comes as a normalization constant. In physical meaning zero range DWBA assumption suggests us that the particle 'b' is emitted at the same point at which particle 'a' is absorbed, so that $r_b = \frac{M_A}{M_B} r_a$ (where A, B are the masses of the corresponding nuclei).

The use of zero range approximation reduces the computation of the six dimensional integral in equations 2.13 or 2.14 into three dimensional integral and the interaction in this representation is represented by delta function (δ) as ; $V_{bx}(r_{bx})\psi_a(r_{bx}) \approx D_0\delta(r_{bx})$, where, D_0 is the asymptotic normalization constant of the wave function of the particle 'a' [Sat02, Sat03].

The spectroscopic factors $S_{\ell,j}$ extracted from the pickup and stripping reactions should follow the sum rule. Pickup with ℓ, j from a target gives the fullness of the orbital while stripping onto the same target indicates the emptyness of the orbital. In case of pickup reactions , $\sum_{J_A} S_{\ell,j}(\mathrm{B,A}) = n(\ell, j)$, where $n(\ell, j)$, is the average no. of nucleons of type x in the ℓ, j shell in the target nucleus. While in the case of stripping, $\sum_{J_A} S_{\ell,j}(\mathrm{A,B}) = (2j+1) - n(\ell, j) = h(\ell, j)$ with $h(\ell, j)$ is the average no. of x-type holes in the (ℓ, j) shell in the target ground state. The sum of $S_{\ell,j}$ for pickup and stripping must be equal to $(2j + 1)$. The detailed discussion for spectroscopic factors can be found in [Sat02, Gle01].

2.1.2.3 Experimental spectroscopic factors

The theoretically predicted cross sections from the DWUCK code and the experimental cross sections were matched to extract the C^2S values for the observed states of the recoil nucleus. Several basic information of the projectile, target, ejectile and product nucleus are used in the DWUCK4 code as inputs to calculate the theoretical cross section. The inputs used in DWUCK4 code are introduced in the next section. The value of the transferred angular momentum and parity of the states can be deduced from the experimental angular distributions; so, single particle states of the product nucleus can be verified. The experimental spectroscopic factors of the observed states of ^{26}Al were extracted using the following relation between experimental and theoretical cross sections taken from [kunz01, Bas01];

$$\left(\frac{d\sigma}{d\Omega}\right)_{exp.} = \frac{NC^2S}{2J+1}\left(\frac{d\sigma}{d\Omega}\right)_{DWBA}, \tag{2.18}$$

where, $(\frac{d\sigma}{d\Omega})_{exp.}$ is the experimental differential cross-section and $(\frac{d\sigma}{d\Omega})_{DWBA}$ is the cross-section predicted by the DWUCK4 code. The value of the constant N is taken from literature and it is 3.33 and 2.95 for (d,t) and (d,^{3}He) reactions respectively. J ($J = \ell \pm \frac{1}{2}$) is the total angular momentum of the orbital from where the neutron or proton is picked up. $C^2$is the isospin Clebsch-Gordon coefficient and its values for the reactions ^{27}Al(d,t)^{26}Al and ^{27}Al(d,^{3}He)^{26}Mg are 1/3 and 2/3, respectively, and S is the spectroscopic factor.

2.1.2.4 Method for DWBA calculation

DWBA calculation has been performed using zero range DWBA (ZR-DWBA) computer code DWUCK4 [kunz01]. Several control parameters have been used while writing the input file and also several input cards have been used in the DWUCK4 code. A short description of control parameters and input cards are available in [kunz01]. First card in DWUCK4 input file includes various control parameters for the programme and controls how the output can be written or suppressed. Second input cards is for initial and final angles with angle step for the calculation. Third input card controls the number of maximum partial waves used in the calculation. The orbital and angular momentum transfer values estimated will be given third input cards which can be estimated using the formulation given in [Sat02]. After third input card , fourth one is used to control the the integration step size, lower and upper cut-off radius and finite range correction factor. After this fifth card is used to give details of the entrance channel as beam energy, mass and charge of target and projectile with spin of the projectile followed by the optical model potential parameters for entrance channel in separate line. After entrance channel inputs, card for final distorted wave inputs is used which requires Q-value for the reaction, mass and charge of ejectile and final nucleus with spin of the ejectile followed by the optical model potential parameters for exit channel in separate line. After entrance and exit channel inputs, a separate input card was designed for transferred particle form factor which needs single particle binding energy,

neutron's mass, charge and spin with mass and charge of the final nucleus followed by separate OMP parameters in separate line in which the well depth was adjusted by the code to get the required separation energy for the transferred particle. After these cards, the details about the orbitals from where the particle was transferred is specified in different card. After all these specific inputs, the last card is used to represents the end of data. The details of the input cards are given in [kunz01].

After calculating theoretical cross sections in ZR-DWBA, Eqn. 2.18 has been used to extract spectroscopic factors for the analysis of all observed states of ^{26}Al and ^{26}Mg. The unceratinty in spectroscopic factor caused by the choice of optical model potential parameters was also examined in this study. Also, we examined the effect of bound state potential parameter in this study. The small examination of the uncertainty that arises using finite range correction parameter along with nonlocal correction parameters was also performed. The detailed calculation and estimation of uncertainties in spectroscopic factors of the observed states of ^{26}Al and ^{26}Mg are given in analysis and result chapter 4.

Chapter 3

Experimental Details and Data Analysis Technique

This chapter consists of several sections, organized in the following manner. Short descriptions of the facilities used in the experiment (the accelerator, scattering chamber and detectors) have been given in section 3.1. Details of the present experiment (Experimental setup, electronics set up, data acquisition and the the particle identification technique) have been described in section 3.2. The details of the data analysis procedure has been given in section 3.3.

3.1 General description of facilities used in the experiment

3.1.1 Accelerator: Variable Energy Cyclotron

The experiment has been performed at the Variable Energy Cyclotron Centre (VECC), Kolkata, India, using the deuteron beam of 25 MeV from K130 cyclotron. The K130 cyclotron is a sector-focused, isochronous cyclotron [Div01] and is shown

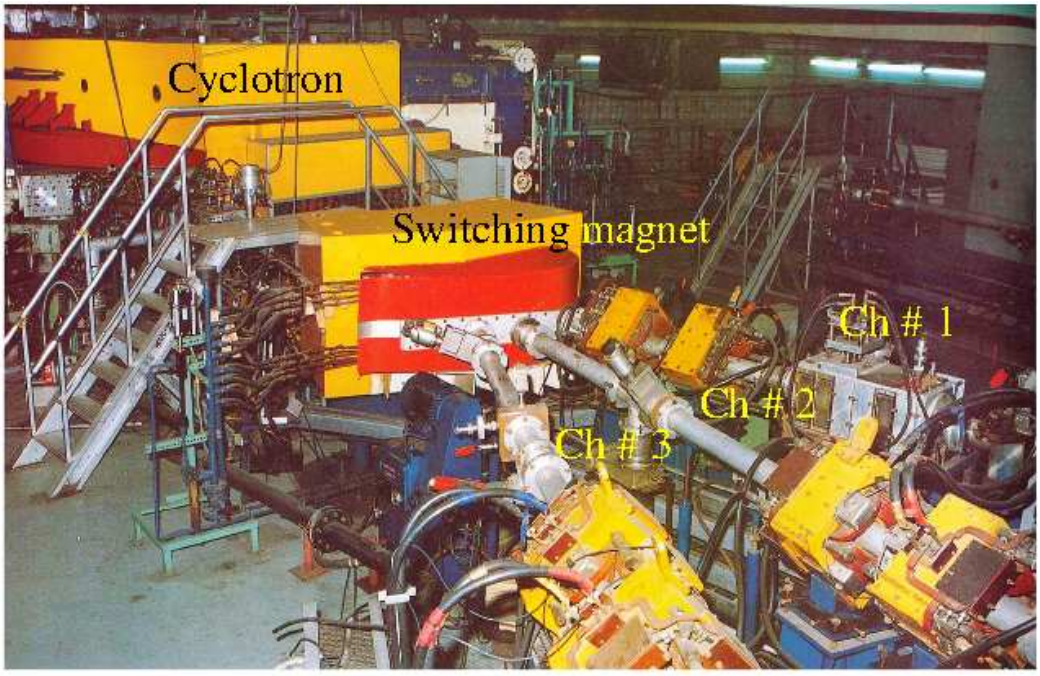

Figure 3.1: K130 Variable energy cyclotron with switching magnet and various beam lines.

in Fig. 3.1. The diameter of the main magnet is 224 cm and it can produce a maximum magnetic field of 2.1 T in the pole gap. Details of the K130 cyclotron parameters are given in Table 3.1. It is able to deliver accelerated light ions beam with the help of Penning Ionisation Gauge (PIG) ion source while using Electron Cyclotron Resonance (ECR) ion source, it can deliver accelerated heavy ions beam. As per design specification, it can accelerate charged particles upto the energy of $130(Q^2/A)$ MeV, where, Q and A are the charge state and the atomic mass of the accelerated particle, respectively. There are four beam line channels corresponding to different types of experimental interest, which are shown in Fig. 3.2. The high current or irradiation experiments were carried out in 0^0 (Ch# 1 in Fig. 3.2) beam line. The second beam line shown as Ch# 2 in Fig. 3.2 is used for charged particle experiments while experiments with γ-detectors as well as charged particle detector are performed in the third beam line (Ch# 3). The fourth beam line in Fig. 3.2 shown by Ch# 4 has been dedicated for radioactive ion beam (RIB) facility.

Table 3.1: Technical specifications of K130 cyclotron.

Cyclotron	
Cyclotron type	:Azimuthally Varying Field (AVF)
Magnet	
Shape of magnet	: H-shaped electromagnet
Pole diameter	: 224 cm
Average pole gap	: 24.5 cm
Average magnetic field	: 17.1 kG (max. of 2.1 T)
Main coil power	: 490 kW
Trim coil power	: 433 kW
Valley coil power	: 27 kW
R. F. System	
Frequency range	: 5.5 - 16.5 MHz
Dee Voltage	: 70 kV (max)
Energy gain	: 140 keV /turn (max)
Oscillator power output	: 300 kW (max)
Ion Source	
Type	: Hot cathode PIG, ECR
Filament current	: 500 A (max)
Arc current	: 0- 2 A
Arc voltage	: 10 - 600 V
Deflector	
Type	: Electrostatic 120 kV (max)
Vacuum	
Operating pressure	: 10^{-6} Torr
Beam	
Energy	: Proton 6 - 30 MeV : Deuteron 12 - 65 MeV : Alpha 25 - 130 MeV : Heavy ion 7-11 MeV/A
Internal beam current	: 100 μA
External beam current	: 20 μA
Extraction radius	: 99 cm
Resolution	: 0.5% (FWHM)
Beam pulse width for particles	: 4 ns

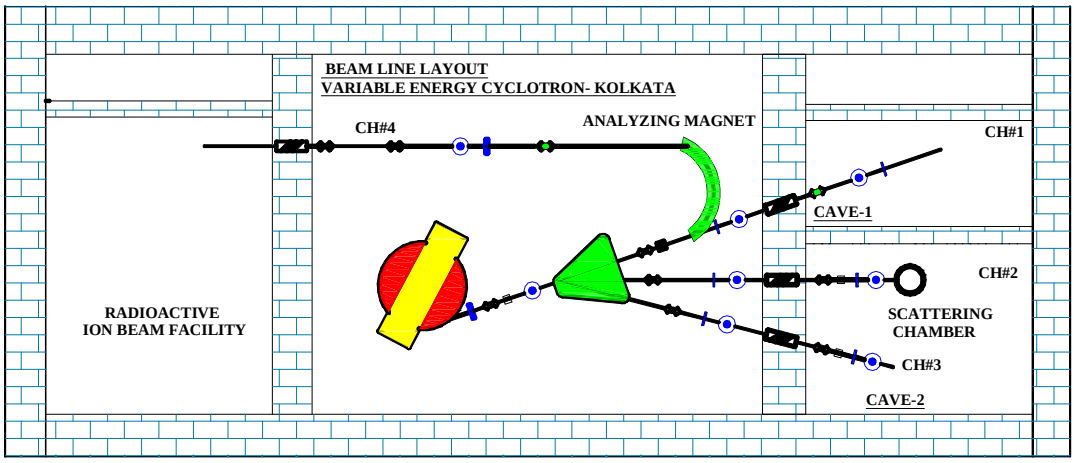

Figure 3.2: Layout of different beam lines of K130-cyclotron.

3.1.2 Scattering chamber

The present experiment was performed in general purpose scattering chamber (GPSC) which is placed in the second beam line (Ch# 2 in Fig. 3.2). The shape of GPSC is cylindrical and its diameter is approximately 1m. On each side of beam direction, there are two rotating arms which can be rotated from outside to cover the required angular range. There are several holes in each arm to put the detector at particular position. The movable target ladder is placed at the centre of the GPSC and it can be controlled from outside. The vacuum (1×10^{-5} mbar) is achieved with the help of a large diffusion pump and rotary pump combination.

3.1.3 Detectors

In the present experiment, a three elements detector telescope made from Si strip (ΔE) - Si strip (E) - CsI(Tl) detector combination was used to detect charged particles. In the following subsections, a general discussion on different types of detectors e.g. (Si and CsI(Tl)) along with the detectors used in the experiment have been given. The detailed characteristic properties about Si and Csi(Tl) detectors can be found in [Knoll,

LeoWR]. The details characteristics of the detectors used in the present experiment is available in [TK01].

3.1.3.1 Silicon detectors

Silicon detectors are very frequently used for detecting charged particles because of their good energy resolution and linear energy response to charge particles. The advantage of semiconductor detector is that the average energy required to create an electron-hole pair is 10 times smaller than that required for gas ionisation. Thus the amount of ionisation for a given energy is an order of magnitude greater resulting in increased energy resolution. Moreover, because of their higher density, they have a higher stopping power than gas detectors. One can segment the contacts of the main detector volume into different section because of the availability of large area silicon wafer. These different sections are called strips and each strip can be used as a separate detector which is referred as silicon strip detector. Depending upon the energy of outgoing particles, detector thicknesses have been chosen so that particle can be stopped in the detectors. One can achieve good position resolution using si strip detectors. The Silicon strip detectors used in the present experiments are ion-implanted, passivated devices obtained from M/S Micron Semiconductors Ltd., UK [UK01]. A brief description of different elements of the detector telescope used in the present experiment has been given below.

3.1.3.2 Single sided Silicon strip detector (SSSD)

The first element (ΔE) of the detector telescope is a SSSD of thickness 55 μm, so as to have low energy threshold for ionizing particle like ^{3}H etc. In the present case Si strip(ΔE) detector can stop ^{3}H of $\approx$ 3.2 MeV and ^{3}He of $\approx$ 7.8 MeV. It is made up of a single silicon wafer having an active surface area of 50$\times$50 mm^{2}. It consists of 16 vertical strips in front side (each of dimension 50 mm$\times$3 mm and in between two consecutive strips 50 mm$\times$0.13 mm separation gap) which are read out individually

and back side is grounded and is shown in Fig. 3.3(a). The resolution of the single-sided Si(ΔE) strip detector was < 70 keV for 5 MeV α - partcle. These detectors can be operated up to two times the typical full depletion voltage(FD) i.e up to 2FD and typical range of FD is 4V to 8V; total leakage current ~20 nA (typical) with maximum 100 nA at 2FD.

3.1.3.3 Double sided Silicon strip detector(DSSSD)

The second element (Si(E)) of the detector telescope is a double sided silicon strip detector of thickness of 1030 μm (shown in Fig. 3.3(a)) can stop ^{3}H of ≈ 19.8 MeV and ^{3}He of ≈ 39.8 MeV. This detector is also made up of a single silicon wafer having active surface area of 50×50 mm^2. Both the sides (Front; vertical side (EF) and back;horizontal side (EB)) of this DSSSD consists of 16 strips (dimension of each strip is 50 mm×3 mm) are mutually orthogonal to each other. Typical full depletion voltage(FD) for theses detectors ranges from 120V to 130V and can be operated up to FD +30 V; total leakage current at FD+30 V is ~6 00 nA (at 25^{0}C) with max. leakage current is 3 μA. The resolution of double sided Si(E) strip detector was < 25 keV for 5 MeV α - particle.

3.1.3.4 CsI(Tl) detectors

The cesium iodide [CsI(Tl)] is an inorganic scintillator detector in which Tl acts as an activator. It is widely used to detect energetic charged particles because of its high stopping power for charged particles and cost effectiveness. The response of the detector is not very linear with energy but is a complex function of not only of energy but of the type of particle and its specific ionisation. The CsI(Tl) is less hygroscopic than NaI(Tl), so it gives very good performance at room temperature. CsI(Tl) is used as charged particle detector in two ways; (I) as a stop (E) detector in ΔE-E telescopic mode, or, (II) as a single detector using its particle discrimination property to detect light charged particles. In the present experiment the third element of the telescope is a

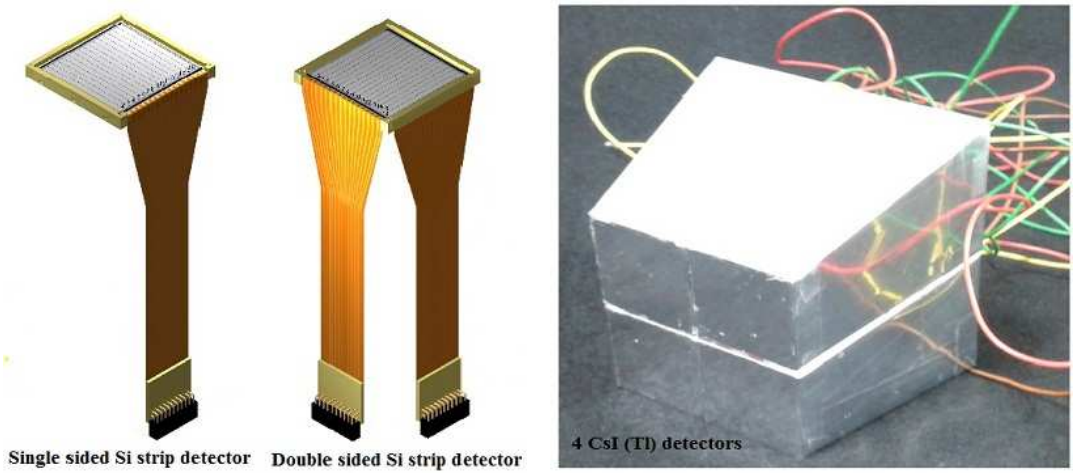

(a) (b)

Figure 3.3: (a)Single sided Si(ΔE) and double sided Si(E) strip detectors and (b) Four CsI(Tl) detector placed on each other.

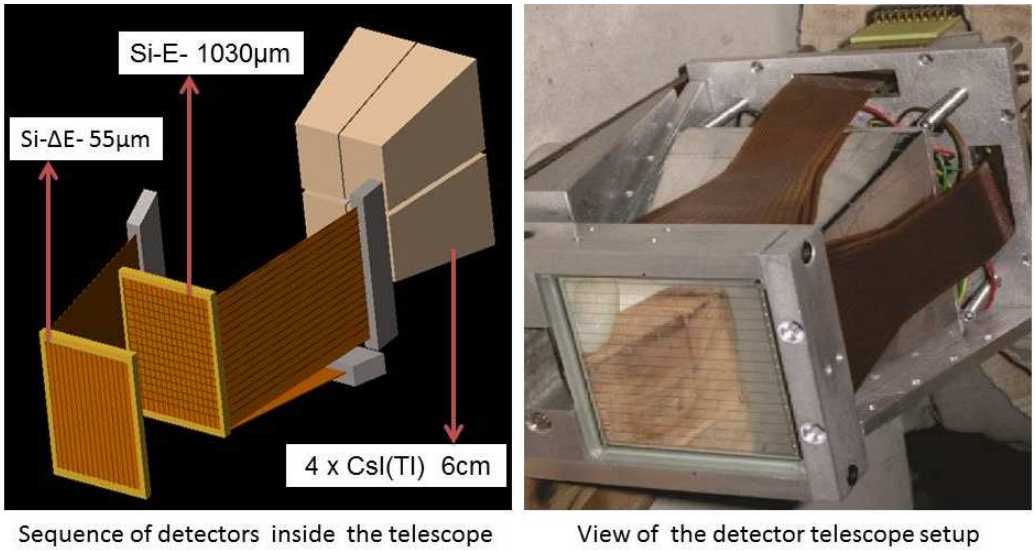

Figure 3.4: A schematic sequence and view of different elements telescope.

stack of four CsI(Tl) detectors (Fig. 3.3(b)), which is used as a stop (E) detector for the energetic particles. The front and back faces of these detectors are square shaped of dimension 2.5 cm × 2.5 and 3.5 cm × 3.5, respectively. The thickness of each CsI(Tl) detector is 6 cm which can stop proton with energy upto ∼ 140 MeV and ^{16}O with energy ∼ 330 MeV/A. Each crystal is coupled with a photodiode (active area of 18 mm × 18 mm) (Hamamatsu S3204-08). The reverse bias voltage that can be applied to photodiode is 100 V (maximum). The range of temperature in which it can be operated is -20^0 to 60^{0}C. A charge sensitive preamplifier (gain of preamplifier is ∼ 5 mV/MeV) is directly coupled with the photodiode and can be operated in vacuume [TK01]. The schematic view and sequence of single and double sided Si strip detectors alongwith the Csi(Tl) detectors to form a telescope is shown in Fig. 3.4.

3.2 Description of the present experiment

3.2.1 Experimental setup

The experiment has been performed using 25 MeV deuteron beam from K130 Variable Energy Cyclotron on a self-supported ^{27}Al (thickness~90 μg/cm^2) target. The experimental set up used in present experiment is shown in Fig. 3.5. A three element telescope has been used for particle identification, details of which has been presented in 3.1.3. A horizontal slit of width 6 mm was placed in front of the telescope and it was kept at a distance of 19.5 cm down stream from the target. The solid angle subtended by each strip was 0.47 msr. The angular distributions of various transfer channels were measured using the above described detector telescope system. Typical two dimensional specta obtained at 28^0 using Si strip(ΔE) - Si strip(E) and Si strip(E) - CsI(Tl) detectors telescope have been shown in Fig. 3.6(a) and Fig. 3.6(b) respectively. The inclusive angular distributions of the ejectiles were measured in the angular range of 16° to 40°. Typical angular resolution of each strip is 0.9^o. Different ridges seen corre-

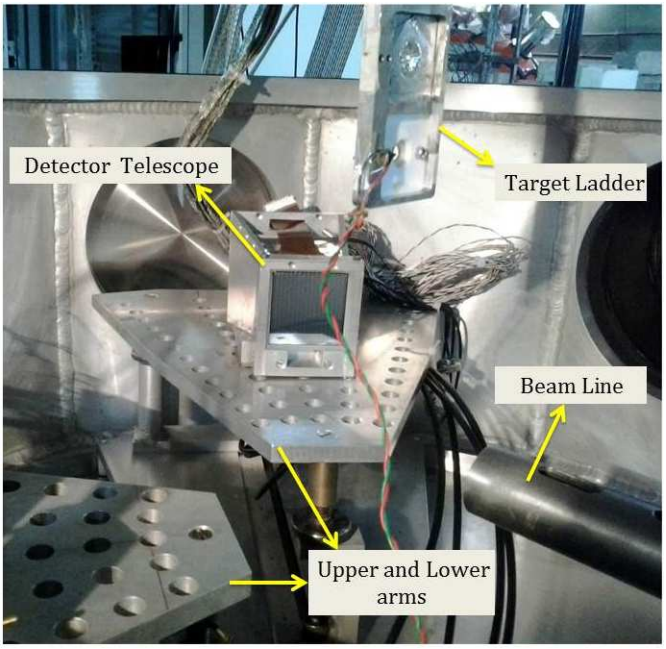

Figure 3.5: Detector telescope setup used in the present experiment.

spond to different outgoing particles produced through the reactions ^{27}Al(d, t), ^{27}Al(d, ^{3}He) and ^{27}Al(d, α) are shown in Fig. 3.6(a).

3.2.2 Electronic set-up and data acquisition

A general discussion of the electronic set-up and data acquisition system have been given in this subsection. The electronic setup used in the present experiment has been shown in Fig. 3.7 and a schematic block-diagram of the electronic setup has been shown in Fig. 3.8. Since each strip detector consists of 16 strips per side, so we have used a custom made 16 channel MPR-16 pre-amplifier and 16 channel MSCF-16 amplifier with differential outputs manufactured by M/s Mesytec Pvt. Ltd, Germany as per our specification to process the signal from the detector. All Strips and the CsI(Tl) detectors were read out individually using standard readout electronics. The signals from the detectors were first fed to the pre-amplifier. The output of the pre-amplifier is a fast rising signal of few miliVolts with a long exponential tail of the order of 50

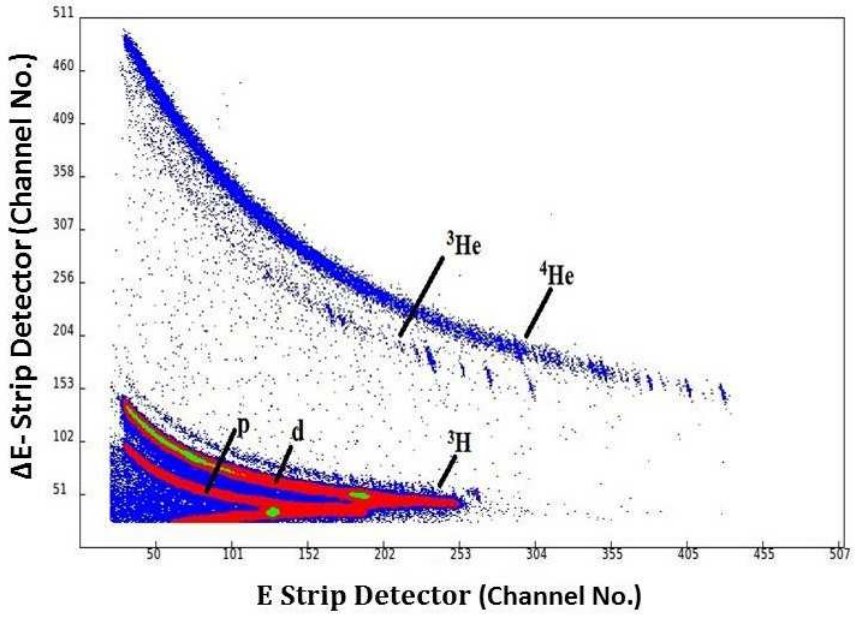

(a)

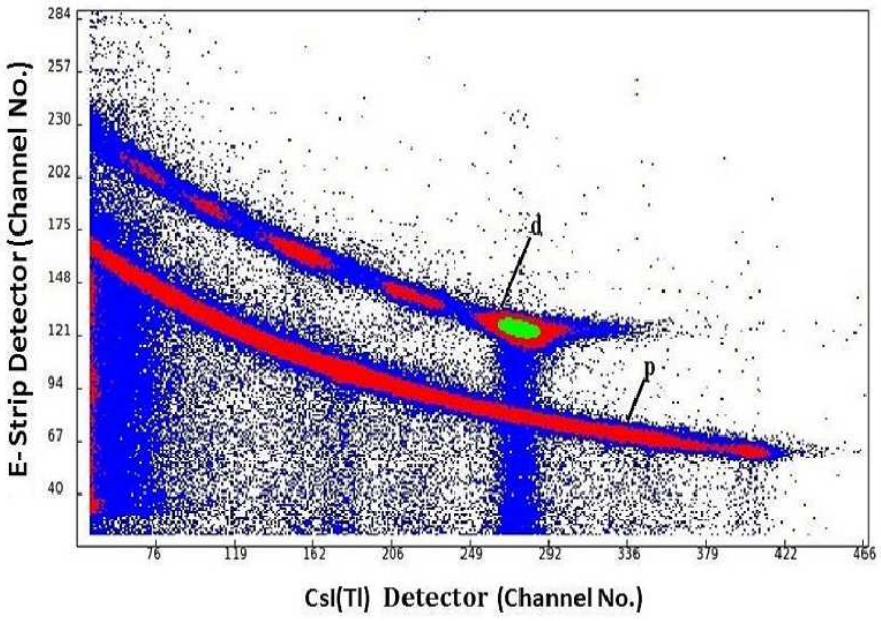

(b)

Figure 3.6: (a)Typical two dimensional spectra obtained using Si(ΔE) strip Vs. Si(E) strip detector telescope and (b) obtained using Si(E) strip Vs. CsI(Tl) detector telescope.

Figure 3.7: The electronic setup used in the present experiment.

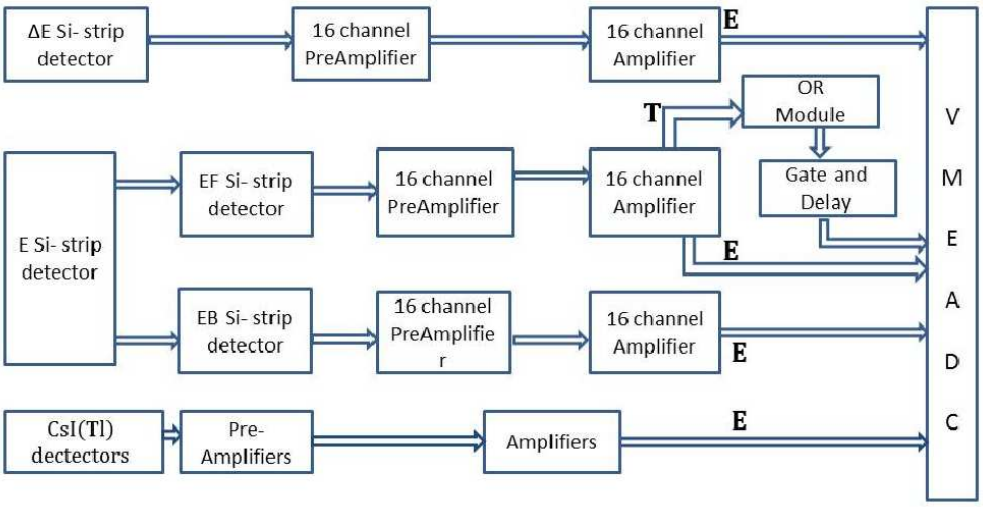

Figure 3.8: Schematic block-diagram of the electronic setup.

μs or more. For further amplification and shaping, the output of the preamplifier is then fed to 16 channel MSCF amplifier. The TFA (Timing-Filter-Amplifier) and CFD (Constant Fraction Discriminator) were in-built in the MSCF-16 amplifier. The TFA and CFD were used for timing and threshold application. The Gaussian shaped output pulse (pulse height ~ a few Volts) from the amplifier was further processed through the 32 channel analog to digital (ADC) (Model CAEN V785) and was stored using Versa-Module Eurocard (VME) data acquisition system (DAQ) developed at VECC. OR-Logic was also generated by these amplifiers. The OR-Logic was used to generate master trigger after some logic operation. A custom made 16 channel shaper with TFA and CFD (MSCF-16, unipolar header input) was used for all CsI(Tl) detectors. All the electronic modules used in the electronic set-up and VME-DAQ system, kept inside the experimental hall, were controlled through Ethernet.

3.2.3 Particle identification technique

As described above, detector telescope setup using Si-strip(ΔE),Si-strip(E) and CsI(Tl) detectors was used in the present experiment for the identitification of different outgoing particles. A short description of the particle identitification method using telescope is presented in this section. We know that the linear stopping power or the specific energy loss for the charged particle in a given material is defined by the following relation:

$$S = -\frac{dE}{dx} \tag{3.1}$$

Where, dE is the differential energy loss for that particle and dx is the corresponding differential path length.

We also know that for particle with a given charge state, S increases with the decrease in the particle velocity. The specific energy loss can be described by Bethe formula as given below [Knoll]:

$$-\frac{dE}{dx} = \frac{4\pi e^4 z^2}{m_0 v^2} NB \tag{3.2}$$

where

$$B = Z\left[ln\frac{2m_0v^2}{I} - ln(1-\frac{v^2}{c^2}) - \frac{v^2}{c^2}\right] \tag{3.3}$$

and v, ze, M are the energy, velocity, charge and mass of the incident particle and N, Z are the number density and atomic number of the absorber (here detector material) and m_0 is the electron rest mass and e is the electronic charge. The parameter, I, represents the average excitation and ionization potential of the absorber and normally treated as an experimentally determined parameter for each element. For non-relativistic particle ($v << c$), only the first term in B is significant. The value of B in general varies slowly with the energy of the incident particle. So, for a given nonrelativistic particle the Eq. 3.1 can be reduced as:

$$-\frac{dE}{dx} \propto \frac{Mz^2}{E} \tag{3.4}$$

When we form two detector telescope, the energy loss in thin detector (ΔE) is very less than the total energy E of the particle and the product ΔE. E becomes constant for a given particle of mass M and charge z and represents the equation of a rectangular hyperbola. The product $\Delta E.E$ is different for different particles but always represents the equation of the rectangular hyperbola for the corresponding particles. So, in the two dimensional spectrum obtained by ΔE Vs. E plot, we get separate rectangular hyperbolas for different particles detected. In this way we identify the particles using detector telescope.

3.3 Offline data analysis procedure

For the analysis of data offline, the standard analysis platform (ROOT) has been used. The data reduction has been done using algorithm developed in ROOT platform to extract the details (angular position (θ), energy, types of particle etc.) of the detected

particle in each event. The details of the offline analysis have been described below in different subsections:

3.3.1 Target thickness measurement

In the present experiment, thickness of ^{27}Al target was measured using a ^{229}Th-α source of five groups of known energies (4.79, 5.82, 6.34, 7.07 and 8.38 MeV). We used a single surface barrier detector with the standard electronic set up to detect the enrgy spectrum of α particles corresponding to energies of the five peaks. To measure the thickness of the ^{27}Al foil, first we measure the energy spectrum with the target foil by placing the target in between the detector and the Th-α source. After this, the measurement of the energy spectrum of α-source has been done without placing the the target foil. After passing through the target, the incident particle losses some energy due to the target thichness, which was calculated from the shift in the ADC channel number observed from the energy spectrum of α particles. Energy calibration of the detector has been done using the known energy peaks of -α particles and the ADC channel number. After energy calibration, the energy loss in the target foil has been calculated from the corresponding shift in the ADC channel numbers. The stopping power (dE/dx) for different energies of α-particle in the target material has been obtained from the code SRIM 2008 [SRIM]. The average thickness of the target was estimated by taking the average of the ratios of energy loss in the target and stopping power corresponding to different α peak energies. The average thickness of ^{27}Al target has been estimated to be ~ 90 μg/cm^2.

3.3.2 Gain match factor

To calculate the total energy of the any fragment, the energy deposited in the Si(ΔE) strip detector and Si(E) strip detector has to be added. To add the energy deposited in these two detectors the gain of Si(ΔE) strip detector and Si(E) strip

detector should be same. For this purpose, in the present study pulser has been used. The signal from pulser has been fed into the test input of the preamplifiers of of Si(ΔE) and Si(E) strip detectors. The two dimensional spectrum obtained from pulser has been used to match the gain of the detectors using the relation E(channel number) = $m_p \times \Delta$E(channel number) + c_p. where, m_p and c_p are the slope and intercepts obtained in the linear fitting of channel numbers of E and ΔE detectors. Typical spectra obtained to get the gain match factors (m_p and c_p) between two different strips of Si(ΔE) and Si(E) strip detectors using pulser have been shown in Fig 3.9. Typical gain match factors m_p and c_p for 3^{rd} strips are 0.203 and 63.849 while for the 12^{th} strips are 0.18973 and 50.05889, respectively. In this way, the gain of all the strips of Si(ΔE) strip detector and Si(E) strip detector are brought in the same scale.

The total energy deposited is proportional to the the total channel number which was obtained by adding the energy deposited in the Si(ΔE) and Si(E) strip detectors. The total channel number was then measured using the relation E_{total}(channel number) = E(channel number) + ($m_p \times \Delta$E(channel number) + c_p) for all the strips of strip detector separately. A typical two dimensional spectrum obtained after gain matching of the 12^{th} strip is shown in Fig. 3.10. Different ridges seen in Fig. 3.10 correspond to different outgoing particles produced in the reactions ^{27}Al(d, t), ^{27}Al(d, ^{3}He) and ^{27}Al(d, α). A typical total energy spectrum (in channel nos.) of ^{3}H obtained by projecting ^{3}H ridge onto the (E + ΔE) axis is shown in Fig. 3.11(a). Different peaks in this spectrum corresponds to different excited states of ^{26}Al populated through the reaction ^{27}Al(d, t). Further this process has been repeated for all strips (16 strips, which correspond to different angles) to obtain the energy spectra of ^{3}H at different angles. Similarly, the total energy spectrum of ^{3}He for different strips (different angles) have been obtained by projecting ^{3}He ridge onto the (E + ΔE) axis. A typical total energy spectrum (in channel nos.) of ^{3}He is shown in Fig. 3.11(b) in which different peaks correspond to different excited states of ^{26}Mg populated through the reaction ^{27}Al(d, ^{3}He). These spectra obtained in channel number in this manner were

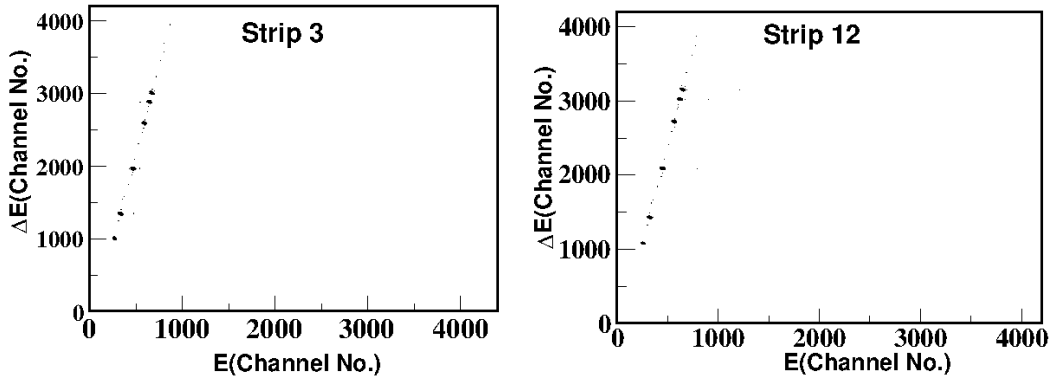

(a) (b)

Figure 3.9: Two dimensional spectra obtained using pulser for the 3^{rd} and 12^{th} strips of Si(ΔE) strip Vs. Si(E) strip detector telescope.

further converted into total energy spectrum after calibration of each strips of the strip detector. The calibration procedure has been described in the following sub section.

3.3.3 Energy calibration of detectors

Seperate calibration has been done to extract energy informations about the observed states of ^{26}Al and ^{26}Mg populated through the reactions ^{27}Al(d, t) and ^{27}Al(d, ^{3}He) respectively. For the ^{3}H, the energy calibration of each strips of the strip detector has been done using the well known states of ^{26}Al (ground, 228, 417, 1058, 2070, 2365, and 2545 keV) while for ^{3}He, the calibration of each strips has been done using well known states of ^{26}Mg (ground, 1808 and 2932 keV) alongwith ground state of ^{26}Al, respectively. For a given strip (for a given angle), the energies of ^{3}H and ^{3}He corresponding to different populated states of ^{26}Al and ^{26}Mg have been obtained using two body kinematics, respectively. Knowing the energies of different peaks from two body kinematics, the channel numbers of the respective peaks (as shown in Figs. 3.11(a) and 3.11(b)) have been calibrated using linear relation Energy(E) = m × channel number + c. where, m and c are the slope and intercepts obtained in the linear fitting. This process was done for all the strips. Typical cali-

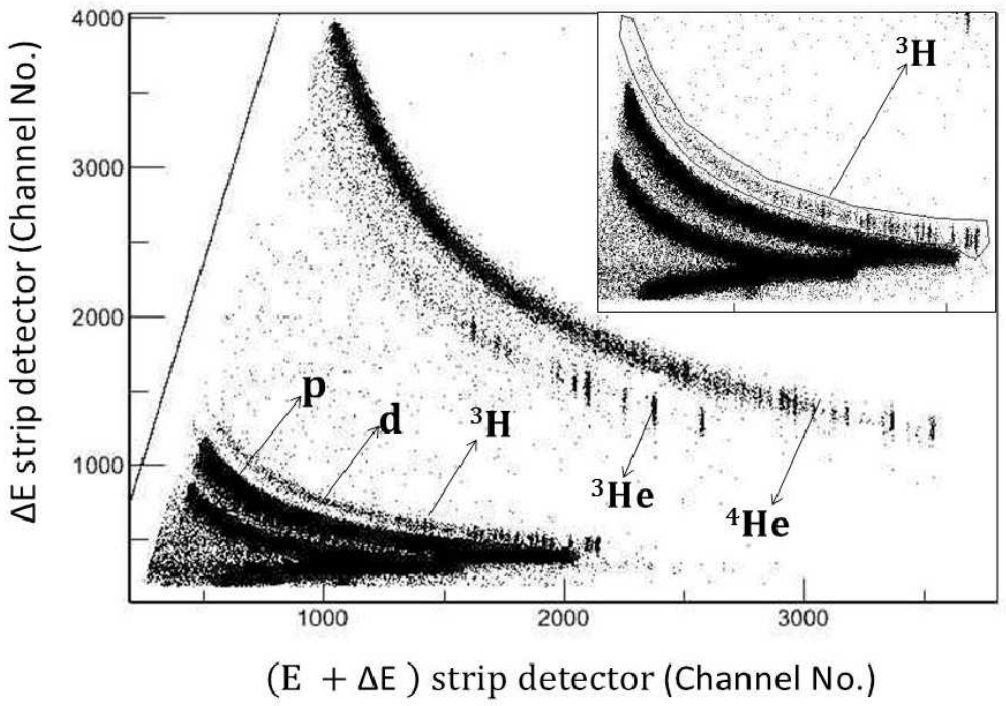

Figure 3.10: Typical two dimensional spectrum obtained after gain matching at $\approx 36^0$.

bration graph for the 3^{rd} and 14^{th} strips of the Si(E) strip detector for ^{26}Al and ^{26}Mg have been shown in Fig. 3.12(a) and Fig. 3.12(b) respectively. Energy calibrations of the CsI(Tl) detectors were done using the two-dimensional spectrum obtained by the Si Strip and CsI(Tl) detectors.

3.3.4 Energy loss corrections

In measuring energies as well as excitation energies, energy loss corrections due to the target thickness and the dead layers in Si detectors were also taken into consideration. The energy loss due to the target thickness and the dead layers in the Si detectors depends on the type of particle detected in the detector. After incorporating all corrections, the corrected energy of the particle can be written as;

$$E_c = E_{detected} + \Delta E_{target} + \Delta E_{detector} \tag{3.5}$$

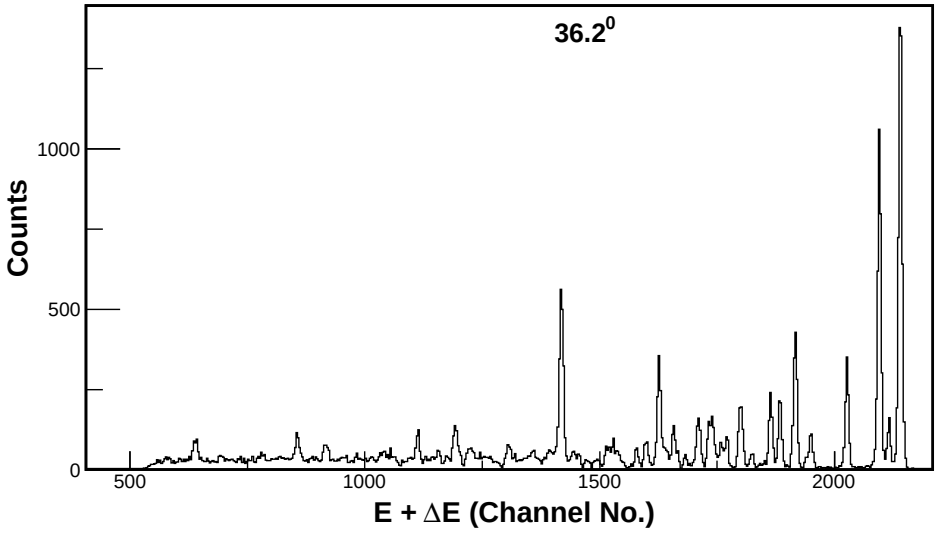

(a)

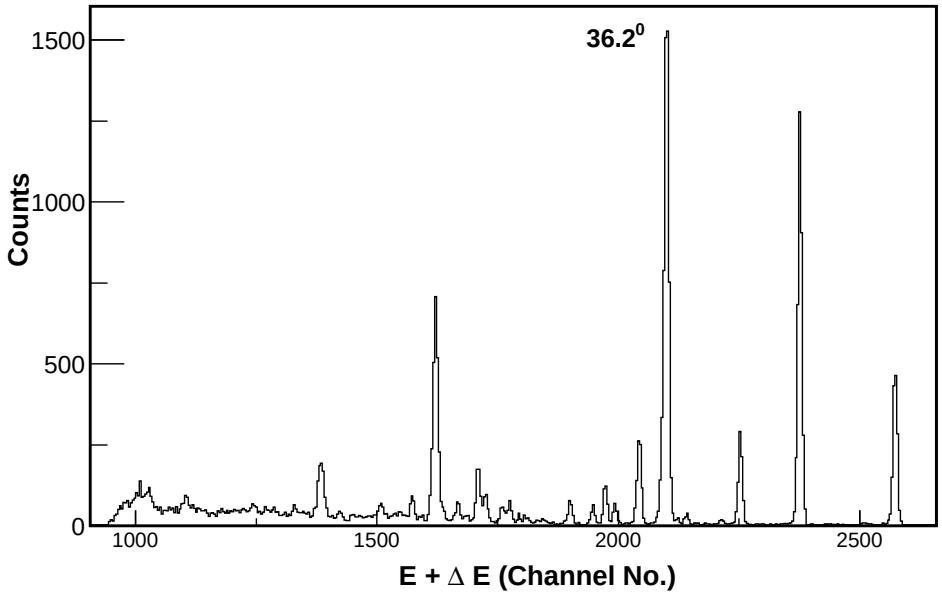

(b)

Figure 3.11: (a) Projection of ^{3}H ridge and (b) Prejection of ^{3}He ridge onto the (E + ΔE) axis at $\approx 36^{0}$.

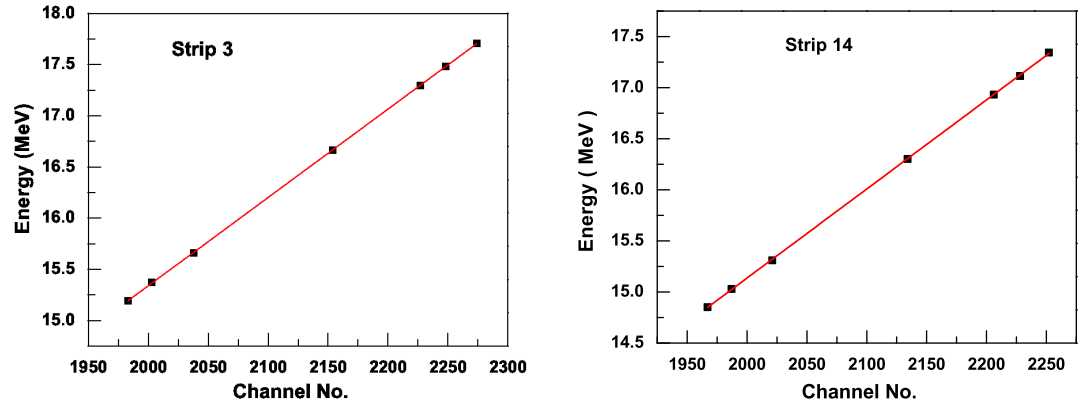

(a)

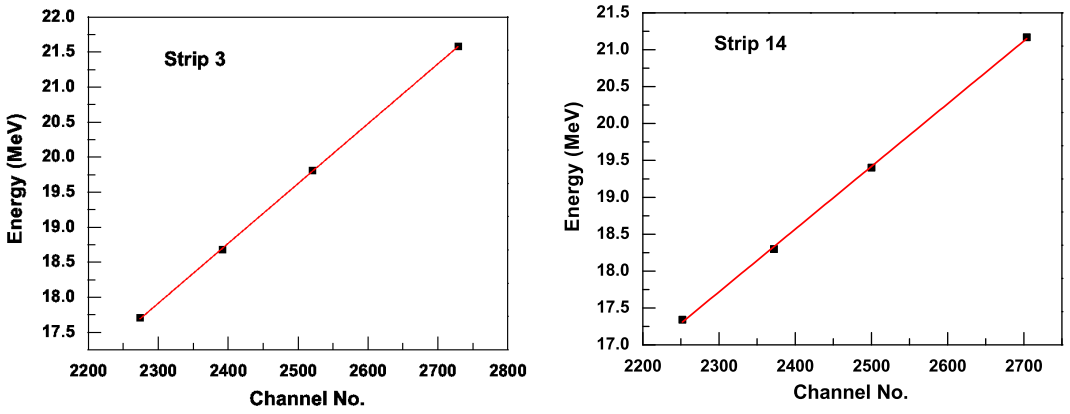

(b)

Figure 3.12: (a) Energy calibration of 3^{rd} and 14^{th} strips of Si(E) strip detector using seven known states of ^{26}Al while (b) represents the enaergy caliberation using three states of ^{26}Mg and ground state of ^{26}Al.

where, E_c is the corrected energy of the outgoing particle, $E_{detected}$ is the energy measured in the detector, ΔE_{target} is the energy loss in target foil and $\Delta E_{detector}$ is the energy loss in dead layer of the detector.

Due to the finite target thickness, it has been assumed that the reaction occurs uniformly over the whole target thickness. So, half thickness (middle) of the target (average point of interaction) was considered to correct the energy loss due to target thickness. ΔE_{target} can be calculated as $(\frac{dE}{dx})\frac{t}{2}\sec(\theta)$, where, $(\frac{dE}{dx})$ is the energy loss in the target material, t the thickness of the target and θ is the angle with respect to the beam direction. In the present work, we used LISE++ [LISE] software and calculated the ΔE_{target} and typical energy loss inside the ^{27}Al target in the present case was from 2 to 3 keV for ^{3}H. The energy loss correction due to dead layer in Si detectors was estimated using the standard thickness of the dead layer provided by the manufacturer. So, in this way different energy loss corrections were incorporated while estimating the energies and excitation energies of the neucli of interest.

3.3.5 Method to generate excitation energy

After calibration of each detector, excitation energy spectrum has been generated for the recoil nucleus at different angles. The excitation energy (Ex) spectrum, was constructed using the following equation:

$$Ex = E_{lab} - (E_B + E_r - Q); \tag{3.6}$$

where, E_{lab} is the energy of incident particle, E_B is the enrgy of the ejectile particle, E_r is the energy of the recoil nucleus. Q is the Q-value for the reaction and its value for the reaction ^{27}Al(d,t)^{26}Al is -6.80 MeV while for the reaction ^{27}Al(d,^{3}He)^{26}Mg is -2.78 MeV.

The overlap of excitation energy spectra corresponding to the observed states of ^{26}Al and ^{26}Mg, obtained at two different angles are shown in Figs. 3.13 and 3.14 respectively. In Figs. 3.13 and 3.14, different excited states of ^{26}Al and ^{26}Mg are clearly

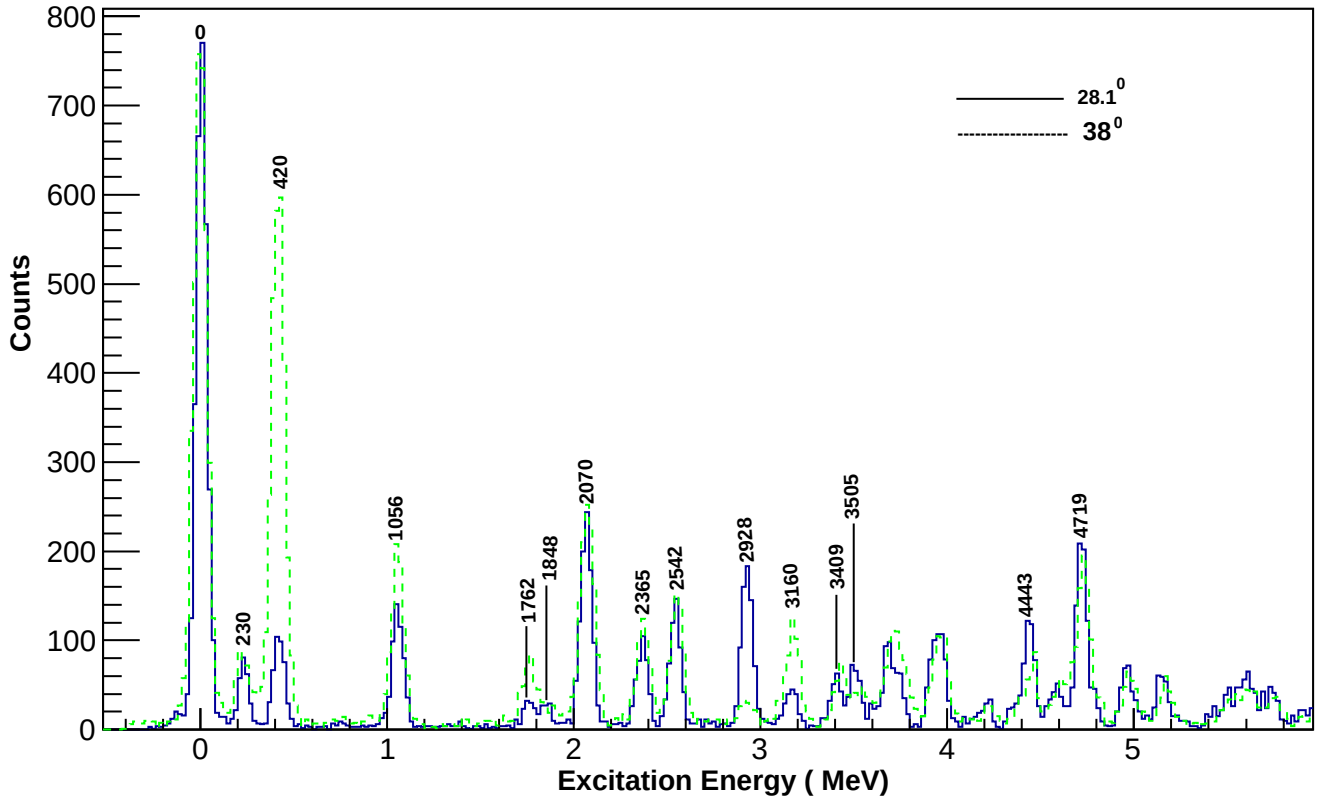

Figure 3.13: Excitation energy spectra of ^{26}Al obtained at $\theta_{lab} \approx 28^{\circ}$ (solid line) and at $\theta_{lab} \approx 38^{\circ}$ (dash-dash). Excitation energies labeled inside the figure are in keV.

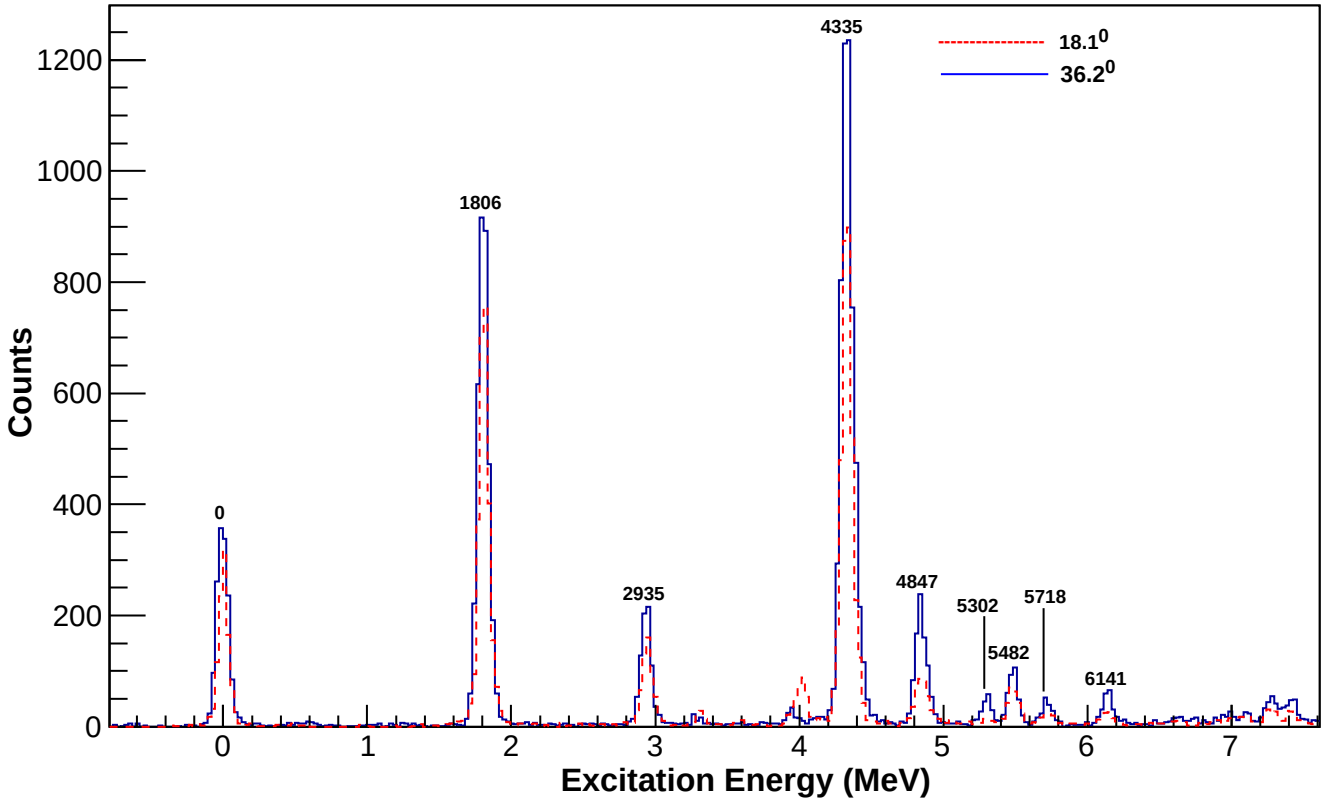

Figure 3.14: Excitation energy spectra of ^{26}Mg obtained at $\theta_{lab} \approx 18^{\circ}$ (dash line) and at $\theta_{lab} \approx 36^{\circ}$ (solid line). Excitation energies labeled inside the figure are in keV.

visible respectively. In this way, the identification of different excited states of ^{26}Al and ^{26}Mg have been done. In the next step, experimental cross sections were extracted for all the observed states which has been described in the following sub section. The analysis of different states has been discussed in chapter 4.

3.3.6 Calculation of experimental cross sections

To get the experimental cross section, the total yield (counts) or area under each peak was extracted. The Faraday cup reading was used to estimate the number of incident particle while target thickness was used to estimate the number of target nuclei taking part in the interaction. Since ΔE and E detectors are Si strip detectors, so in Si -Si telescope system, there are cross talks among the different strips of ΔE and E detectors apart from one to one correspondence. So, in the present analysis, the cross talk events were also considered and were added in the yields (counts) or total area for the different observed states. Finally, the experimental cross section was estimated using the following equation,

$$\left(\frac{d\sigma}{d\Omega}\right)_{exp.} = \frac{Y}{N.I.d\Omega} \tag{3.7}$$

where,

$\left(\frac{d\sigma}{d\Omega}\right)_{exp.}$ → the experimental cross section,

Y → the total area under the peak,

N → the number of target nuclei per unit area which is estimated using the relation, $N = \frac{N_A}{A}t$, where, A, N_A and t are atomic mass of the target, Avogadro number 6.023×10^{23} atoms/mol and thickness of the target respectively.

I → the number of incident particle per second and it is measured from the total collected charge in Faraday cup.

dΩ → solid angle subtended on the detector.

Since in Si - Si telescope system the protons and elastically scattered deuterons would pass through in the Si(E) detector and get fully stopped in the CsI(Tl) detector. So, the elastic scattering cross section was extracted using the combination of Si strip

and CsI(Tl) detectors. In the present study, the ratio of elastic scattering cross section to Rutherford cross section was calculated. The said ratio was further used to extract optical model potential parameter and the method to extract optical model potential parameters were described in chapter 4. The extracted optical model parameters were used in the analysis of transfer reaction study and the detailed analysis was described in chapter 4.

The cross sections in lab frame calculated using above eqn. 3.7 was converted into centre of mass (CM) frame to interpret in theoretical predictions as follows [Ren01];

$$\left(\frac{d\sigma}{d\Omega}\right)_{CM} = \left(\frac{d\sigma}{d\Omega}\right)_{Lab} \frac{\mid 1 + \gamma \cos(\theta)_{CM} \mid}{(1 + \gamma^2 + 2\gamma \cos(\theta)_{CM})^{\frac{3}{2}}} \tag{3.8}$$

Where, $\gamma = \left(\frac{A1.A3}{A2.A4}\frac{E_{cm}}{E_{cm}+Q}\right)^{\frac{1}{2}}$, in which A1, A2, A3, A4 are the masses of the projectile, target, electile and recoil nucleus while E_{cm}, Q and $(\theta)_{CM}$ are the center of mass energy, Q-value of the reaction and angle in center of mass system respectively.

The error in cross section data was taken to be the total error in the present study. Total error includes systematic as well as statistical errors. The systematic error included the uncertainties in the target thickness measurement, the Faraday cup reading and the solid angle measurement. The statistical error was calculated with the area or total number of counts (N) under the peak, which is $\frac{1}{\sqrt{N}}$. In the present work each type of the systematic errors were taken to be 5%. Finally, all the estimated errors have been incorporated by adding them in quadrature and taking the squareroot of the quadrature addition to estimate the total error in the experimental data points.

Chapter 4

Results and Discussions

The main aim of the present thesis work is the experimental study of the observed states of ^{26}Al and ^{26}Mg populated through the reactions ^{27}Al(d,t) and ^{27}Al(d,^{3}He) respectively. So, in this chapter, discussions about the extracted spectroscopic factors of the observed states of ^{26}Al and ^{26}Mg have been presented. The details of the experiment performed to fulfil the aim of the present thesis work were already discussed in chapter 3. This chapter has been divided into two major sections which are further divided into different subsections to discuss the results extracted from the present thesis experiment. The first section of this chapter (section 4.1) contains the study of the reaction ^{27}Al(d,t) which is the first direct study of ^{26}Al using (d,t) reaction channel. Zero-range distorted wave Born-approximation (ZR-DWBA) calculations was performed to extract the spectroscopic factors for fourteen observed states of ^{26}Al populated through the single neutron transfer reaction ^{27}Al(d, t) and relative spectroscopic factors were compared with those reported earlier using other single neutron pick up reactions [Kro01, Shw01, Bet01, Nur01]. The second section of this chapter (section 4.2) deals with the study of ^{27}Al(d,^{3}He) reaction. Nine observed states of ^{26}Mg populated through ^{27}Al(d,^{3}He) reaction were studied by ZR-DWBA calculations and the extracted values of spectroscopic factors were compared with the same obtained earlier [Ver01, Wil01, Wag01, Ard01]. We also compared the spectroscopic factors

of the observed low lying T=1 (ground, 1806 and 2935 keV) states of ^{26}Mg with the corresponding T=1 states studied in the present study of ^{27}Al(d,t) reaction [vish01].

For the above purpose, each section of this chapter has been arranged in following manner; starting from the optical model analysis, DWBA calculation, methods used to estimate spectroscopic factors and finally results and discussions about the observed states of ^{26}Al and ^{26}Mg sequencely.

4.1 Analysis of the reaction ^{27}Al(d, t)

4.1.1 OMP parameters for the entrance channel (d+^{27}Al).

In the present work [vish01], the optical model search code ECIS94 [Ran01] was used to extract the optical model potential parameters for the entrance channel d+^{27}Al. The elastic scattering cross sections of 25 MeV deuteron were measured in the angular range of 16° to 40° in steps of 0.9 ° using the combination of Si strip and CsI(Tl) detectors of the detector telescope discussed in chapter 3. The experimental angular distribution of the cross sections of elastically scattered deuterons from ^{27}Al target obtained in the present study alongwith the 23 MeV elastic scattering data taken from [Mah01] have been shown in 4.1 and these were fitted using the optical model search code ECIS94 using phenomenological optical model potential in the parametric Wood Saxon (WS) form for both real and imaginary potentials in the optical model analysis.

Three sets of optical model potential parameters were extracted for d+^{27}Al in the entrance channel which are consistent in the description of the measured elastic angular distribution. Search of the OMP parameters set A (given in Table 4.1) was initiated with volume real, surface imaginary and spin-orbit potential parameters taken from [Uda01]. For other two sets (set B and set C given in Table 4.1), the optical model potential parameters given in [Wil01] were used as the initial parameters to

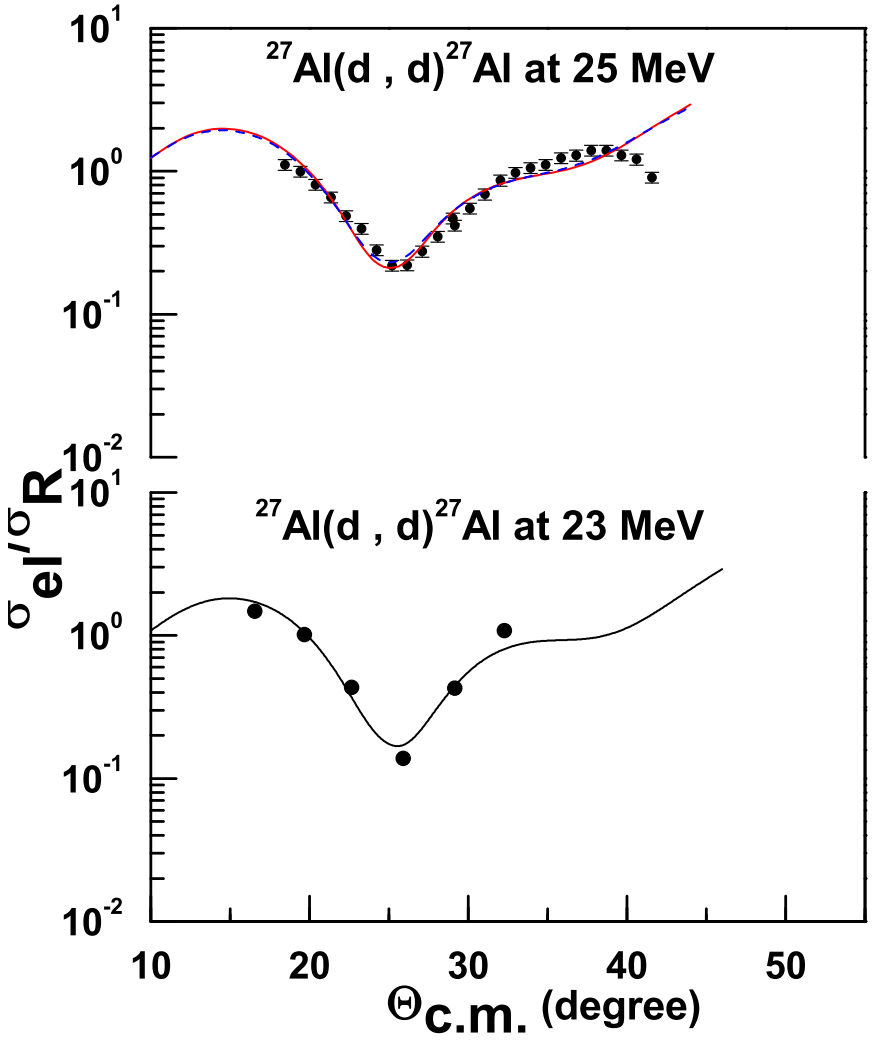

Figure 4.1: Angular distributions of elastically scattered deuteron from ^{27}Al at E_{lab} = 25 MeV (present data) and 23 MeV. The filled circles represent experimental data, solid and dash-dash lines represent optical model fits for set A and set B, respectively.

search for suitable OMP parameters for the d+^{27}Al system at 23 MeV. Initially, the elastic scattering cross section data of 23 MeV deuterons from ^{27}Al target taken from Ref. [Mah01] has been fitted. The best fit potential parameters of the 23 MeV elastic scattering data ((set C in Table 4.1) were subsequently used as the starting parameter set for fitting 25 MeV elastic scattering data of the present experiment. The final parameter values are given as Set B in Table 4.1. All the parameters were varied to arrive at the minimum χ^2 per degree of freedom, χ^2/N_f. The best fit potential parameters corresponding to minimum χ^2/N_f are listed in Table 4.1. The χ^2 may be defined as;

$$\left[\chi^2 = \sum_{i=1}^{N_f} \frac{(\sigma^{exp}(\theta_i) - \sigma^{th}(\theta_i))^2}{(\Delta\sigma^{exp}(\theta_i))^2}\right]. \tag{4.1}$$

Where, N_f is the total number of experimental data points, θ_i is the scattering angle, $\sigma^{th}(\theta_i)$ and $\sigma^{exp}(\theta_i)$ are the theoretical and experimental cross sections and $\Delta\sigma^{exp}(\theta_i)$ is the corresponding error in the experimental cross sections, respectively. The optical model fits to the elastic scattering data are displayed in Fig. 4.1 for both sets (A and B) of potential parameters. The values of χ^2 are almost same between the two sets, but the total reaction cross sections differ by ~10%.

4.1.2 OMP parameters for t+^{26}Al in exit channel.

Several sets of optical model potential parameters in the exit channel were tried but only a few of them were found to be suitable to reproduce the experimental cross sections of the observed states of ^{26}Al. Finally, two sets of optical model parameters for the t+^{26}Al exit channel were chosen. The first set (A1 in Table 4.1) was obtained from the relation given in Perey and Perey [Per01] and the second set (B1 in Table 4.1) was taken from [Trib01] for the ^{28}Si(d,t) reaction.

Table 4.1: The best fit potential parameters used in DWUCK4 code for ^{27}Al(d,t) reaction.

Reaction	Set	V (MeV)	R_o (fm)	a_o (fm)	W_v (MeV)	W_D (MeV)	R_I (fm)	a_I (fm)	V_{ls} (MeV)	R_{ls} (fm)	a_{ls} (fm)	R_C (fm)
d+^{27}Al	A	89.209	1.061	0.701		2.250	1.360	0.850	9.00	1.061	0.801	1.25
	B	90.301	1.055	0.675		2.407	1.400	0.850	9.00	1.055	0.780	1.25
	C	88.095	1.055	0.780		3.524	1.300	0.650	9.00	1.055	0.780	1.25
t+^{26}Al	[a]A1	161.91	1.200	0.720	39.99		1.40	0.840	2.50	1.20	0.720	1.30
	[b]B1	172.0	1.140	0.710	17.52		1.670	0.780				1.30
[c]n+^{26}Al			1.200	0.650								1.30

[a] Parameters extracted from the relation given in Perey and Perey [Per01].

[b] Parameters taken from ^{28}Si(d,t) [Trib01].

[c] Well depth adjusted to get the required separation energy for the transferred particle.

Table 4.2: Extracted C^2S values for different states of ^{26}Al for the reaction ^{27}Al(d,t).

[a)]Ex(keV)	J^π	ℓ	[b)]Ex(keV)	C^2S
0	5^+	2	0	0.73±0.21
228.3	0^+	2	230	0.09±0.03
416.8	3^+	2	420	0.32±0.07
		0	420	0.07±0.03
1057.7	1^+	2	1056	0.17 ±0.05
1759.0	2^+	2	1762	0.038±0.006
1850.6	1^+	2	1848	0.019±0.004
2068.8	2^+	2	2070	0.26±0.06
2365.1	3^+	2	2365	0.13±0.02
2545.3	3^+	2	2542	0.16±0.03
3159.8	2^+	2	3160	0.06±0.01
3402.6	5^+	2	3409	0.06±0.01
3507.6	6^+	4	3505	0.06±0.03
4430.7	2^-	1	4443	0.23 ±0.04
4705.3	4^+	2	4719	0.27±0.08

[a] Values taken from the NNDC [Nnd01], [b] Present work and uncertainties in Ex in present work are within ± 10 keV

4.1.3 DWBA Calculation for the reaction ^{27}Al(d, t)

The experimentally extracted angular distributions of the observed states of ^{26}Al populated through ^{27}Al(d,t) reaction are shown in Figs. 4.2 to 4.7 by solid points and these were fitted with the respective theoretical predictions from computer code [kunz01]. In the present thesis work, full zero-range distorted wave Born approximation calculation has been performed to extract spectroscopic factors of the observed states of ^{26}Al. The optical model potential parameters given in Table 4.1 have been used in the DWBA calculation. The J^π assignments of the states, displayed in corresponding figures were taken from NNDC [Nnd01].

A short description of the input parameters used in DWUCK4 code was already introduced in chapter 2. In this work, the DWBA calculation was performed by assuming pick-up from the $0d_{5/2}$ (ℓ = 2, J = 5/2) single particle orbital for most of the states while by assuming pick up from the $1s_{1/2}$ (ℓ=0, J = 1/2) and $0p_{1/2}$ (ℓ = 1, J = 1/2) single particle orbital was also done for one state for each. The states of ^{26}Al were analysed upto 5.50 MeV of excitation energy. The shapes of the experimental angular distributions were found to be reproduced quite well by the theoretical predictions for states upto 3.409 MeV except for the state at 420 keV. The deviations are comparatively low for lower excited states and gradually increase for higher excited states. The favourable value of the transferred angular momentum was calculated for each and every observed states of the recoil nucleus separately using the relation prescribed in [Sat02]. After calculating the favourable ℓ-transfer in the reaction different inputs corresponding to each of the observed states of ^{26}Al were used to extract the theoretical predictions of the cross sections for each state. The theoretically predicted cross sections were compared with the respective experimental angular distributions to extract spectroscopic factors using zero range DWBA. The relation given in chapter 2 as Eqn. 2.18 between experimental and theoretical cross sections was used in the present study to extract spectroscopic factors.

4.1.4 Methodology used to extract C^2S

The angular distributions of different excited states of ^{26}Al have been analyzed with all the potential sets given in Table 4.1. We used six combinations of the potential parameters, e.g., A-A1, B-A1, C-A1, A-B1, B-B1 and C-B1 to extract the spectroscopic factors and these six sets were also used to estimate the uncertainties in spectroscopic factors. The variations in the extracted spectroscopic factors among the potential combinations A-A1, B-A1 and C-A1, and those among the combinations A-B1, B-B1 and C-B1, were found to be less than 10%. To extract the spectroscopic factor of each state, two sets of average spectroscopic factors were computed; one set was obtained from

the average of the spectroscopic factors for each state calculated with three combinations (A-A1, B-A1 and C-A1) of potential parameters and the other set obtained in the same way from the other three combinations (A-B1, B-B1 and C-B1) of potential parameters. Finally, the spectroscopic factor of each state was taken to be the mean of the corresponding average spectroscopic factors of the two sets. The extracted values of the spectroscopic factors for different excited states have been given in Table 4.2. The deviation between the mean spectroscopic factor and the individual spectroscopic factor for different excited states was found to be less than 20%. The deviations calculated from the two sets of average spectroscopic factors and the average errors in experimental data points were used to estimate the uncertainties in C^2S for different excited states of ^{26}Al. A comparison of these spectroscopic factors with the previously reported values for the same obtained from other reactions is made in Table 4.3. Keeping in mind the uncertainty in the absolute normalization between different reaction probes, the spectroscopic factors for different excited states of ^{26}Al relative to that of its ground state, C^2S/C^2S_{gs} were used for comparison(see Table 4.3).

4.1.5 Results and discussions of the study of the reaction ^{27}Al(d, t)

The angular distributions were analyzed for both sets of exit channel parameters in combination with all sets of entrance channel (set A, set B and set C). In the shell model configuration picture of ^{27}Al with 13 protons and 14 neutrons has ground state spin $5/2^+$. The ground, 230, 1056, 1762, 1848, 2070, 2365, 2542, 3160, 3409 and 4719 keV states of ^{26}Al were studied by assuming pick up from $0d_{5/2}$ single particle orbital. The excited states at 3509 and 4443 keV were studied by assuming pick up from $0g_{9/2}$and $0p_{1/2}$ single particle orbitals, while the analysis of 420 keV state was performed for both $1s_{1/2}$ and $0d_{5/2}$ single particle orbitals. The experimental angular distributions of cross sections of these states are shown in Figs. 4.2 to 4.7 along with the respective theoretical predictions. The theoretical predictions have been found to

reproduce the forward angles data quite nicely indicating the one step process for most of the states.

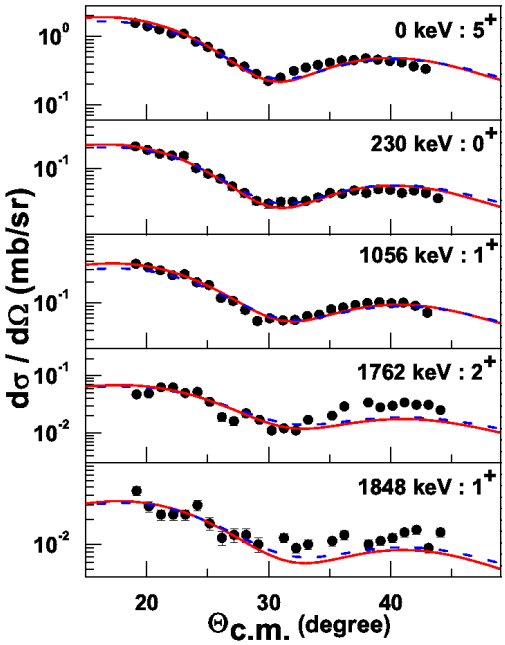

Figure 4.2: Comparison of experimental and theoretical angular distributions for the ground, 230, 1056, 1762 and 1848 keV states. Filled circles are the present experimental data. Solid and dash-dash lines are theoretical predictions from DWUCK4 code for pick up from $0d_{5/2}$ with set A-A1 and set A-B1, respectively.

The angular distribution of ground state (5^+) shown in Fig 4.2 is analysed by assuming pick-up from $0d_{5/2}$ single particle orbital. The spectroscopic factor (shown in Table 4.2) for this state was found to be less compared to that reported using other reactions [Kro01, Bet01]. However, it is in good agreement with the theoretically predicted value for the same (1.0 and 0.61, using two different model configurations) [Kro01].

For the 230 (0^+) and 1056 (1^+) keV states shown in Fig 4.2, the spectroscopic factors were also calculated by assuming pick up from $0d_{5/2}$ single particle orbital and are given in Table 4.2. The spectroscopic factors are found to be in good agreement with the values reported earlier [Kro01, Bet01]. Relative spectroscopic factors were found to be in close agreement with previously reported values. In addition, the C^2S value

obtained for the 230 and 1056 keV states are in good agreement with the corresponding theoretical prediction given in [Kro01]).

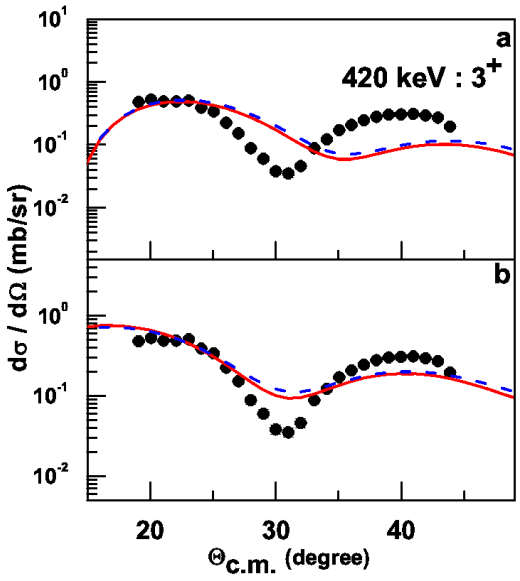

Figure 4.3: Same notations as in Fig. 4.2 for the 420 keV state . The upper plot (a), represents calculation for pick up from $1s_{1/2}$ and lower plot (b), represents calculation for pick up from $0d_{5/2}$.

The angular distribution for the 420 keV state shown in Fig. 4.3 is analyzed by assuming pick up from both $1s_{1/2}$ and $0d_{5/2}$ single particle orbitals separately without considering mixture of these two single particle orbitals. It is clear from Fig. 4.3 that shape of the experimental angular distribution and the corresponding DWBA prediction are in good agreement for an $\ell = 2$ transfer, while it is not so for an $\ell = 0$ transfer. It was earlier indicated that this state was populated with pure $\ell = 0$ transfer [Kro01, Bet01]. However, from the present study we conclude that it resembles more closely with an $\ell = 2$ transfer, rather than an $\ell = 0$ transfer. But the spectroscopic factor obtained from the present study (given in Table 4.2) is comparable with its previously reported value for $\ell = 0$ transfer as well as the respective theoretical predictions [Kro01].

Table 4.3: Comparison of C^2S/C^2S_{gs} of the present study with those obtained from other experimental studies done using different reaction probes for different states of ^{26}Al.

[a)]**Ex(keV)**	ℓ	(present)[a]	[Kro01]	[Shw01]	[Bet01]	[Nur01],b
0	2	1	1	1	1	1
230	2	0.12	0.15	0.14	0.14	0.15
420	2	0.44		0.05		
	0	0.09	0.18	0.15	0.12	0.12
1056	2	0.24	0.24	0.31	0.31	0.29
1762	2	0.05	0.07	0.02	0.02	
1848	2	0.03	0.05	0.016	0.02	
2070	2	0.35		0.52	0.50	
2365	2	0.18	0.28	0.23	0.26	
2542	2	0.22	0.28	0.30	0.30	
3160	2	0.08	0.12	0.10	0.10	
3409	2	0.09	0.19	0.09	0.08	
3505	4	0.08		0.04		
4443	1	0.32		0.02	0.02	
4719	2	0.37	1.00	0.71	0.86	

[a] Present work, The state at 4443 keV is 4437 and 4430 keV in [Bet01] and [Shw01] respectively. The state at 4719 keV is reported as 4711 and 4705 keV in [Bet01] and [Shw01], respectively.

[b] Values of C^2S/C^2S_{gs} for (d,t) reaction were taken from [Vla01]

The angular distributions for 1762 keV (2^+) keV and 1848 keV (1^+) states shown in Fig. 4.2 are not reproduced well with respective theoretical predictions. This may be due to fluctuation in experimental data because of low statistics or may be a mixture of *s* and *d* orbitals. In this work, these two states are analysed by assuming pick-up from $0d_{5/2}$ single particle orbital. The shapes of the angular distribution of these states are in close resemblance with the shape predicted theoretically for $0d_{5/2}$ single particle orbital. The extracted C^2S values (given in Table 4.2) are in good agreement with the previously extracted values as well as with the theoretically predicted values [Kro01].

The angular distribution for 2070 keV :2^+ states is shown in Fig. 4.4. Around the excitation energy of 2070 keV :2^+, there are three states at 2068, 2069 and 2071 keV. These states could not be resolved in the present experiment. The analysis was performed assuming a single state at the average excitation energy of 2070 keV. The spectroscopic factor was subsequently extracted for this state with $\ell = 2$ assuming pick up from $0d_{5/2}$ single particle orbital and are given in Table 4.2. The model calculation reproduced the experimental angular distribution quite well as shown in Fig. 4.4.

The 2365 :3^+ and 2542 :3^+ keV states were analysed using pick-up from $0d_{5/2}$ single particle orbital only unlike the case of the 420 keV (3^+) state, where analyses were done for both $\ell = 2$ and $\ell = 0$ transfers. This is primarily due to the fact that the angular distributions for 2365 and 2542 keV states are found to be well reproduced by $\ell = 2$ transfers (see Fig. 4.4). The spectroscopic factors given in Table 4.2 for 2365 keV and 2542 keV states were also found to be less in the present (d,t) reaction study compared to those obtained using other pick-up reaction probes. The relative spectroscopic factors of these two states are found to be in good agreement [Shw01]. This points to the uncertainty in the normalization of different reaction data. The spectroscopic factor value for the 2542 keV state from this experiment is large compared to its theoretically predicted value [Kro01].

The spectroscopic factor for 3160 :3^+ keV state given in Table 4.2, is also calculated assuming pick-up from $0d_{5/2}$ single particle orbital and is found to be comparable

with its previously calculated value. The 3409 keV :5^+ state of ^{26}Al is also analyzed with pick-up from $0d_{5/2}$ single particle orbital and the shape of the angular distribution at forward angle is quite reproduced by theoretical predictions (see Fig. 4.4). The relative spectroscopic factor for 3409 keV state is in agreement with previously reported vaues for the same as well as with the corresponding theoretical prediction given in [Kro01].

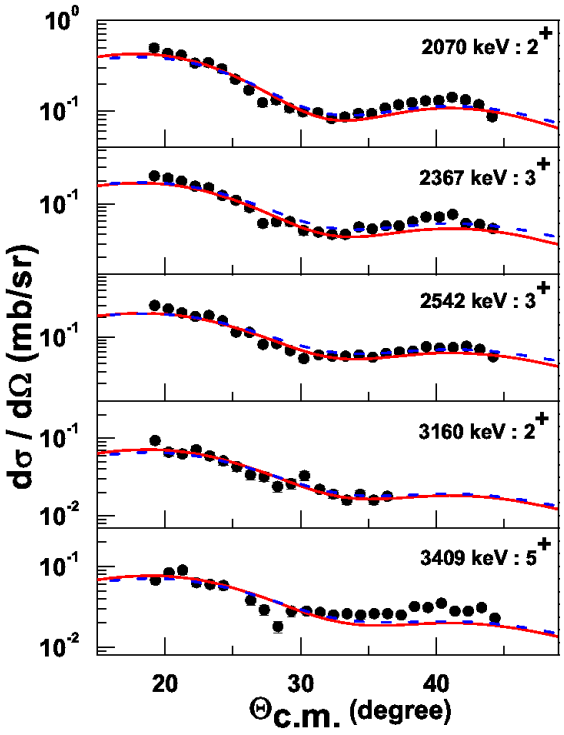

Figure 4.4: Same notations as in Fig. 4.2 for the 2070, 2367, 2542, 3160 and 3409 keV states for pick up from $0d_{5/2}$.

The angular distribution of the 6^+ state does not conform to either $\ell = 2$ or $\ell = 0$ one-step pick up from the s-d shell. One-step transfer requires a pick up from a $0g_{9/2}$ orbital corresponding to $\ell = 4$. This indicates a possible two-step mechanism for excitation of 6^+ state at 3505 keV (see [Kro01]). In this paper, this state was analysed assuming pick-up from a $0g_{9/2}$ single particle orbital and the corresponding DWBA angular distribution is shown in Fig. 4.5. The spectroscopic factor for the state at 3505

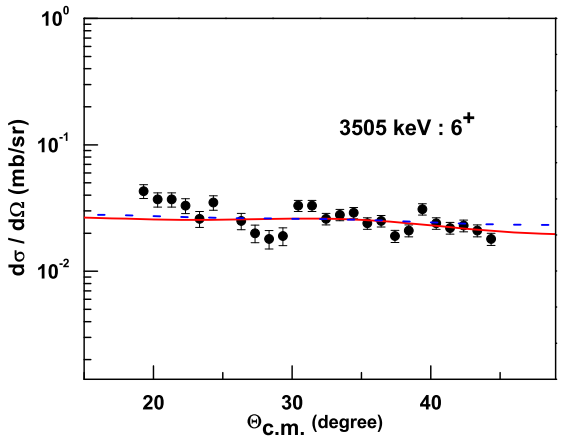

Figure 4.5: Same notations as in Fig. 4.2 for the 3505 keV state for pick up from $0g_{9/2}$.

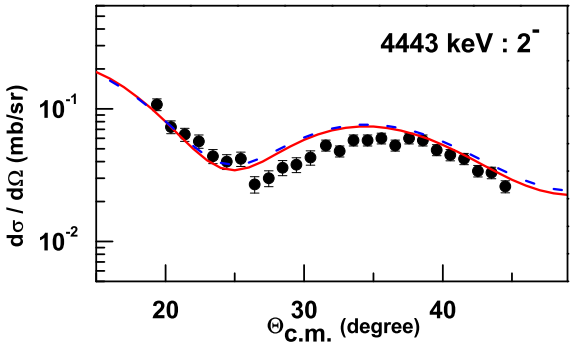

Figure 4.6: Same notations as in Fig. 4.2 for the 4443 keV state for pick-up from $0p_{1/2}$.

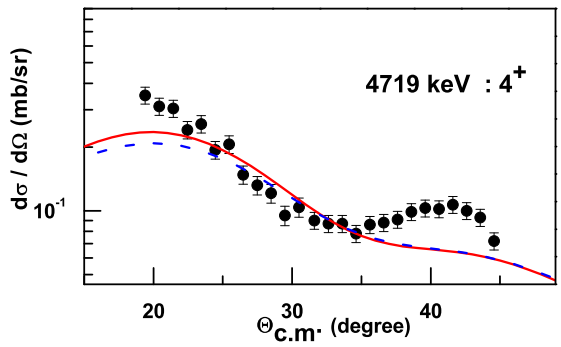

Figure 4.7: Same notations as in Fig. 4.2 for the 4719 keV state for pick up from $0d_{5/2}$.

keV given in Table 4.2 was not reported in [Kro01] and [Bet01]; however, the relative spectroscopic factor given in [Shw01] is in good agreement with the present result assuming pick up from the $0g_{9/2}$ orbital. The fitting is not good.

The shape of the angular distribution at 4443 keV state matches for theoretical predictions for $\ell = 1$ transfers. For this state, the analysis is performed by assuming pick-up from $0p_{1/2}$ single particle orbital closer to the fermi level. In the case of the 4443 keV : 2^- state, there may be mixing of two states; so, the centroid position was considered to extract the C^2S value. For this state (4443 keV : 2^-) the nature of the measured angular distribution shown in Fig. 4.6, was found to match with the corresponding DWBA prediction for pick up from $0p_{1/2}$ orbit. The spectroscopic factor extracted for this state in the present case (shown in Table 4.2) is found to be quite different from the value reported in [Bet01].

The 4719 keV : 4^+ state is analyzed assuming pick-up from $0d_{5/2}$ single particle orbital and it may also be due to the mixing of two states. So, for this state too the determined centroid position was considered to extract the spectroscopic factor. The extracted angular distribution along with theoretical prediction for $\ell = 2$ is shown in Fig. 4.7) and the spectroscopic factor is given in Table 4.2.

In the present work, attempt was also made to extract C^2S using the finite range correction value of 0.845 and nonlocal parameters 0.54, 0.25 and 0.85 for deuteron, tritium and neutron respectively. The fitted angular distributions for two states of ^{26}Al using these parameters are shown in Fig. 4.8; corresponding C^2S values were found to be reduced by 20-50% for the combination A-A1, and by 25-45% for the combination A-B1. The states with poor statistics results large uncertainties in the estimated C^2S values, so the range of estimated uncertainties may be varying to some extent. Because of this reason, we attempted to give the uncertainties in a range from minimum to maximum. The results of the present work can be found in [vish01, vish02, vish03, vish04]. The comparison of extracted spectroscopic factors using a normalization of $N = 2.54$ as used in [Trib01] with a finite range parameter of 1.36 fm^{-1} for (d,t)

reaction given by Hering et al. [Her01] alongwith nonlocal parameters with those with full ZR-DWBA using the OMP sets B and A1 (given in Table 4.1) has also been done and the result can be found in [vish04].

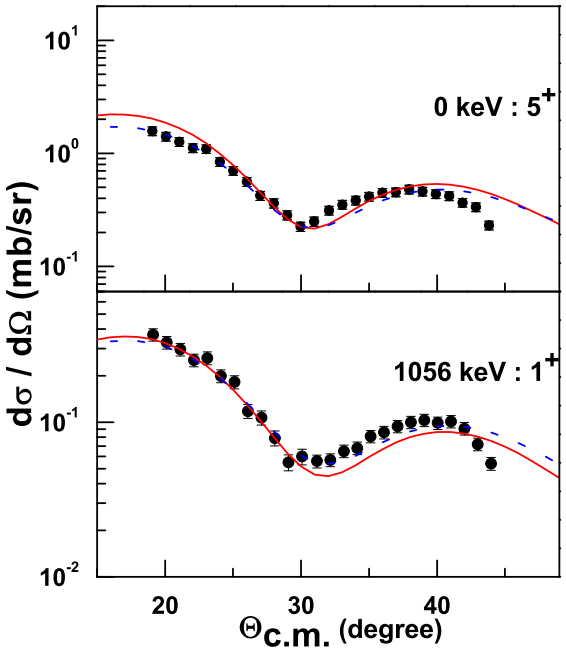

Figure 4.8: Same notations as in Fig. 4.2 for the ground and 1056 keV states but theoretical predictions from DWUCK4 code for pick up from $0d_{5/2}$ includes finite range and non local corrections.

4.2 Analysis of the reaction ^{27}Al(d, ^{3}He)

4.2.1 OMP parameters for ^{3}He+^{26}Mg in exit channel.

Several set of potential parameters available in the literature were tried to fit the extracted experimental angular distributions of the states of ^{26}Mg but only a few sets are found suitable to reproduce the angular distributions. Finally, we selected two sets

of the OMP parameters for ^{3}He+^{26}Mg reaction in the exit channel which are given in Table 4.4 as set B and set C. The OMP parameter set B was calculated using the relation given in Ref. [Per01] while set C was selected from Ref. [Ver01]. The t+^{26}Al parameters Set given in Table 4.1, which was calculated using the relation given in Ref. [Per01] was also tested in the present analysis for ^{3}He+^{26}Mg and this parameter set was also found to reproduce the experimental data nicely. The final set of potential parameters used for the analysis of the extracted cross sections of the observed states of ^{26}Mg populated through the reaction ^{27}Al(d,^{3}He) are given in Table 4.4.

4.2.2 DWBA calculation for the reaction ^{27}Al(d, ^{3}He)

The analysis of different observed states of ^{26}Mg follows the same procedure as used in the analysis for the states of ^{26}Al. The optical model potential parameters used in the DWBA calculation to study the ^{27}Al(d, ^{3}He) have been given in Table 4.4. The experimental angular distributions of cross sections of the observed excited states of ^{26}Mg are shown in Figs. 4.9 and 4.10 and these were fitted with theoretical predictions in ZR-DWBA using the computer code DWUCK4. Spin and parity assignments of the observed states of ^{26}Mg were taken from NNDC [Nnd02].

In this work, the DWBA calculation was performed by assuming pick-up from the $0d_{5/2}$ (ℓ = 2, J = 5/2) and $1s_{1/2}$ (ℓ=0, J = 1/2) single particle orbitals. In addition, analysis of some of the observed states was also performed assuming the configuration mixing of $0d_{5/2}$ and $1s_{1/2}$ single particle orbitals. The favourable value of the transferred angular momentum was calculated by the same manner as discussed in case of ^{26}Al. Different input files corresponding to the different states of ^{26}Mg have been prepared for DWBA calculation to extract the theoretical predictions of the cross sections for each state. The theoretically predicted cross sections were compared with the respective experimental angular distributions to extract spectroscopic factors using zero range DWBA. The relation (Eqn. 2.18) between experimental and theoretical

Table 4.4: The best fit potential parameters used in DWUCK4 code for ^{27}Al(d,^{3}He) reaction.

Reaction	Set	V	R_o	a_o	W_v	W_D	R_I	a_I	V_{ls}	R_{ls}	a_{ls}	R_C
		(MeV)	(fm)	(fm)	(MeV)	(MeV)	(fm)	(fm)	(MeV)	(fm)	(fm)	(fm)
d+^{27}Al	A	89.209	1.061	0.701		2.250	1.360	0.850	9.00	1.061	0.801	1.25
^{3}He+^{26}Mg	B	151.97	1.20	0.720	37.75		1.400	0.880	2.50	1.20	0.720	1.30
	C	217.6	1.15	0.636	32.5		1.319	0.986				1.40
p+^{26}Mg		V	1.20	0.650								1.25

Set A Parameters were taken from present study. [vish01].

Set B were extracted from the relation given in Perey and Perey [Per01] .

Set C Parameter sets were taken from ^{27}Al(d,^{3}He) [Ver01].

V, the Well depth adjusted to give the required separation energy for the transferred particle.

cross sections given in chapter 2 was used in the present study to extract spectroscopic factors.

4.2.3 Calculation of the C^2S values

Spectroscopic factors of the observed excited states of ^{26}Mg were extracted for all the two sets of exit channel potentials (set B and set C) in combination with set A given in Table 4.4. The process of extraction of C^2S values is almost same as adopted in case of ^{26}Al but the estimation of uncertainty in the C^2S values is a little bit different. The detailed process is as follows;

To extract C^2S values for different excited states of ^{26}Mg, the two combinations A-B and A-C of OMP parameters obtained from the entrance-exit channel potential parameter sets given in Table 4.4. The variation in the extracted spectroscopic factors between the potential combinations A-B and A-C, was less than 25% for ℓ= 2 transfer (It should be noted that the variation includes all the observed states for which configuration mixing $0d_{5/2}$ + $1s_{1/2}$ was considered and also for those states which were analysed without configuration mixing). This variation for the ℓ= 0 transfer for the states shown in Fig. 4.9 is large (maximum upto 67%) because of very low contribution as compared to ℓ= 2 transfer while for the states shown in Fig. 4.10, the variation was found to be from 14% to 30%. The average of the extracted C^2S values for different excited states of ^{26}Mg from the said two combinations was taken as final and are given in Table 4.5. The estimated deviations between the C^2S values extracted individually from the combinations A-B and A-C were used in determining the uncertainties in the C^2S values for different excited states of ^{26}Mg. The theoretically predicted C^2S values from the shell and rotational models given in [Wag01, Ard01] are also included in Table 4.5 for comparison. The result of the present analysis can be found in [vish05, vish06, vish07].

The uncertainties in the C^2S values that arise due to the choice of bound-state potential parameters in the calculation of ZR-DWBA, were also taken into consideration to determine the uncertainties in C^2S values in the present study. To see the effect of radius of bound-state potential, we extracted C^2S values for the two afore said OMP combinations using R_o=1.25 fm and taken the average of the C^2S values for all the states. The difference between the average C^2S values calculated using the radius of bound-state potential R_o=1.25 fm and average using R_o=1.20 fm as described above keeping other parameters unchanged was also included in the uncertainty in C^2S values of the observed states of ^{26}Mg. The reduction in the C^2S values for R_o=1.25 fm was approximately 5 to 25% as compared to that with R_o=1.20 fm for ℓ= 2 transfer while for ℓ= 0 transfer, 15% to 40% reduction in C^2S values were noticed except for the states at 1806 and 2935 keV(For these two states, it was found to be increased by 50%).

Along with the above two types of differences estimated in the calculation of C^2S values, the average error in experimental data points was also included in the uncertainty of C^2S values for different excited states of ^{26}Mg. The total uncertainty calculated has been listed in Table 4.5 along with the measured C^2S values for different excited states of ^{26}Mg. So, to reduce the effect of absolute normalization due to the choice of optical model potential parameters and other parameters that can affect the C^2S value, we calculated the relative spectroscopic factors (keeping ground state spectroscopic factor to be 1) for different excited states of ^{26}Mg and compared our results with previously reported values [Ver01, Wil01, Wag01, Ard01] using the same reaction probe. The relative spectroscopic factors are listed in listed in Table 4.6.

It is clear from Table 4.5 that the C^2S values extracted for the states of ^{26}Mg shown in Fig. 4.9 were very large for ℓ= 2 transfer as compared with ℓ=0 transfer in $0d_{5/2}$ + $1s_{1/2}$ configuration mixing. So, for ℓ=0 transfer, the uncertainties were not shown for the states shown in Fig. 4.9 and also we may avoid configuration mixing for these states but for the sake of completeness we presented the results assuming configuration

mixing. For the states shown in Fig. 4.10, the contribution of C^2S values extracted for ℓ= 0 transfer has increased as compared with the states shown in Fig. 4.9.

4.2.4 Results and discussions of the findings of the reaction ^{27}Al(d,^{3}He).

The experimental angular distributions for different excited states of ^{26}Mg produced in the present study of the ^{27}Al(d,^{3}He)reaction at 25 MeV have been fitted with theoretical predictions from the ZR-DWBA computer code DWUCK4. The theoretical predictions were found to reproduce the experimental data well for lower excited states but for higher excited states the deviations between theoretical predictions and experimental data were found to be large at backward angles. The theoretical predictions are found to fit the data good at forward angles, indicating direct process. The detailed dicussion of the present study is given below;

The angular distribution of ground state: 0^+ of ^{26}Mg (shown in Fig. 4.9) is analysed for $0d_{5/2}$ single particle orbital. The theoretical predictions are found to fit the data quite fairly at forward angles. The extracted C^2S value for ground state (give in 4.5) was found to be less in the present study; however, it is consistent, within the limits of uncertainties, with previously reported values using same reaction probe at different energies.

The angular distribution of the 1806 keV: 2^+ state (shown in Fig. 4.9) is analyzed for both $0d_{5/2}$ and $1s_{1/2}$ single particle orbitals. From the angular distribution of 1806 keV shown in 4.9, it is clear that the angular distribution is dominated by $\ell = 2$ transfer. The contribution of $1s_{1/2}$ was found to be <1% as compared with the contribution of $0d_{5/2}$ single particle orbital in the C^2S value and mixing of $1s_{1/2}$ orbital can be neglected. In the present analysis C^2S value of the 1806 keV state (give in Table. 4.5) was also found to be less than compared with the previously reported experimental values given in [Ver01, Wil01, Wag01, Ard01] but the relative C^2S value (give in 4.6)

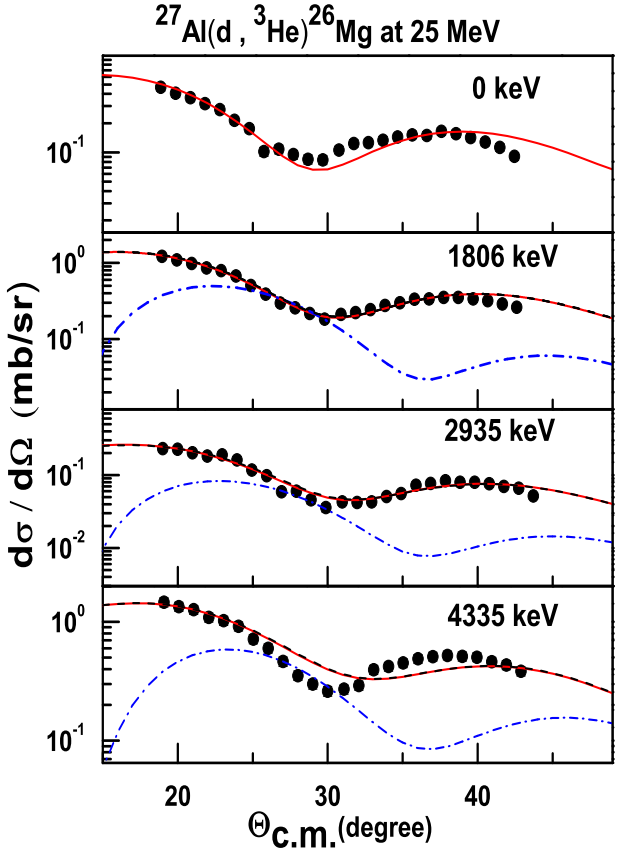

Figure 4.9: Angular distributions for ground, 1806, 2935 and 4335 keV states.The filled circles represent experimental data points and solid line represents theoretical cross section from DWUCK4 code for the OMP combination A-B for considering pick up from $0d_{5/2}$ only, dash-dot-dash represents theoretical cross section for A-B with pick up from $1s_{1/2}$ only while dash-dash represents the theoretical cross sections for $0d_{5/2}$ + $1s_{1/2}$ mixing. Note that theoretical cross sections were normalized to experimental data points.

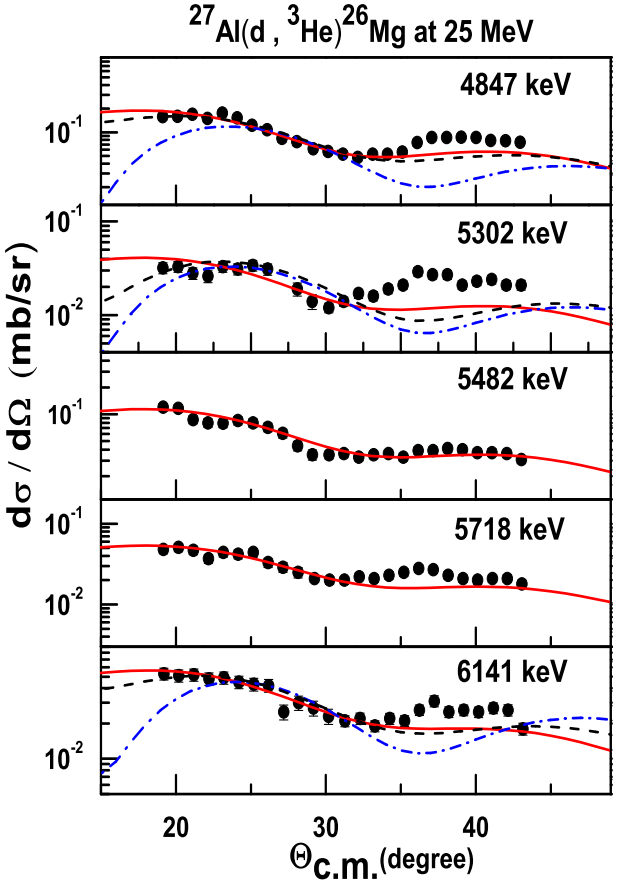

Figure 4.10: Angular distributions for 4847, 5302, 5482, 5718 and 6141 keV states (same notations as in Fig.4.9).

Table 4.5: Extracted values of C^2S for different excited states of ^{26}Mg from the reaction ^{27}Al(d,^{3}He) at 25 MeV.

[a)]Ex (keV)	J^π	[b)]Ex (keV)	[b)]C^2S ℓ=0	[b)]C^2S ℓ=2	⋆TC1 ℓ=0	⋆TC1 ℓ=2	†TC2 ℓ=0	†TC2 ℓ=2
0	0^+	0		0.17 ±0.05	....	0.29	.....	0.33
1808.7	2^+	1806	0.002	0.57 ±0.14	0.014	0.75	0	0.60
2938.3	2^+	2935	0.002	0.13 ±0.03	0.0032	0.29	.....	....
4318					....	.....	.....	0.07
4332	$(2\text{-}4)^+$	4335	0.004	1.03±0.19	....	1.80	≈ 0	0.50
4350					0.16	0.002	≈ 0	0.14
4835.1	2^+	4847	‡0.011±0.010	0.11±0.02	0.0061	0.022	≈ 0	0.36
5291.7	2^+	5302	0.011±0.004	0.011±0.004	.....	0.018	....	....
5476.1	4^+	5482		0.112±0.024	.....	0.025	....	....
5715.6	4^+	5718		0.05±0.006	.....	....	....	....
6125.5	3^+	6141	‡0.011±0.007	0.043±0.005	.....	....	....	....

[a] Values taken from the NNDC [Nnd02].

[b] Present work in which the uncertainties in Ex are within ± 15 keV

⋆TC1 represents theoretical predictions from shell model in [Wil01, Wag01].

†TC2 represents theoretical predictions from rotational model given in [Wag01]..

‡Due to uncertainty in data the reported uncertainties are large.

Table 4.6: Comparison of C^2S/C^2S_{gs} of the present study with those obtained from other experimental studies done using same reaction probe at different energies for different states of ^{26}Mg.

[a)]Ex (keV)	ℓ	(present)[a]	[Ver01]	[Wil01]	[Wag01]	[Ard01]
0	2	1	1	1	1	1
1806	2	3.35	3.33	3.56	3.44	3.34
2935	2	0.76	0.73	0.77	0.70	1.11
4335	2	6.06		7.10	7.15	8.19
4847	2	0.65	0.27	<0.53		
5302	2	0.06	0.04			
5482	2	0.66	0.70	0.80	1.19	0.96
5718	2	0.29	0.23			
6141	2	0.25	0.24	0.4		

[a] Represents the values listed in Table 4.5 (Present work).

was found to be in agreement with previously reported values. It is also found to be in agreement with the rotational model predictions given in [Wag01].

The angular distribution of the 2935keV : 2^+ state (shown in Fig. 4.9) is also analyzed for both $0d_{5/2}$ and $1s_{1/2}$ single particle orbitals. Like the 1806 keV state, also from the angular distribution of 2935 keV, it is clear that the angular distribution is dominated by $\ell = 2$ transfer. The contribution of $1s_{1/2}$ was found to be <1% in the C^2S value as compared with the contribution of $0d_{5/2}$ ((see Table. 4.5) single particle orbital and mixing of $1s_{1/2}$ orbital can be neglected. The relative C^2S value (give in Table. 4.6) for ℓ= 2 transfer is in agreement with the previously reported values while that for ℓ= 0 transfer is comparable with the value reported in [Wag01].

Around the excited state at 4335 keV $(2\text{-}4)^+$ (shown in Fig. 4.9, there are 4318 keV, 4332 keV and 4350 keV excited states and in the present study these states could not be resolved (as shown in Fig. 3.14). So the analysis was performed by taking the

centroid position and C^2S value (give in Table. 4.5) for the 4335 keV excited state was extracted. The spectroscopic factor for the 4335 keV state was found to be less in the present study. The fit is not good.

The angular distribution of 5302 keV: 2^+ state (shown in Fig. 4.10) was analyzed taking mixing of *s* and *d* single particle orbitals. Almost 50% contribution of *s* and *d* orbitals is found in the C^2S value to reproduce the experimental angular distribution. The extracted C^2S value (give in Table. 4.5) for the state at 5302 keV was found to be in good agreement with previously reported experimental value in [Ver01] for both ℓ= 2 and ℓ= 0 transfers and also in good agreement with theoretical predictions from shell model given in [Wil01, Wag01].

The angular distribution of 5482 keV: 2^+ state (shown in Fig. 4.10) was analyzed assuming pick-up from $0d_{5/2}$ single particle orbital only. The extracted C^2S value (give in Table. 4.5) for the 5482 keV state was also less in the present study and its relative C^2S value was compared with previously reported experimental values as well as with predictions from shell model given in [Wil01, Wag01]. It was found that its relative C^2S (give in Table. 4.6) is in agreement with the values reported in Ref. [Ver01, Wil01].

The angular distribution of the 6141 keV : 3^+ state (shown in Fig. 4.10) is analyzed for both $0d_{5/2}$ and $1s_{1/2}$ single particle orbitals and is shown in 4.10. The contribution of $1s_{1/2}$ was found to be 25% of the contribution of $0d_{5/2}$ single particle orbital in the C^2S value. The extracted C^2S value (give in Table. 4.5) for the 6141 keV state was found to be in agreement with the previously reported value in [Ver01] for ℓ= 2 and ℓ= 0 transfers. The relative C^2S value (give in Table. 4.6) of 6141 keV state was found to be in good agreement with previously reported values.

There may be mixture of two or three states in 4847 keV state (shown in Fig. 4.9) but we have taken them together as a single state and the reported excitation energy corresponds to the centroid position. Similarly, there may be mixture of two states in the state at 5718 keV (shown in Fig. 4.9). For 4847 and 5718 keV states, the extracted C^2S value (give in Table. 4.5) were compared with the spectroscopic fac-

Table 4.7: Comparison of spectroscopic factor S of T=1 analog states observed in the reactions ^{27}Al(d,t)^{26}Al and ^{27}Al(d,^{3}He)^{26}Mg at 25 MeV.

$^{a)}$Ex (keV)	$^{(a)}C^2S$	J^π	$^{b)}$Ex (keV)	$^{(b)}C^2S$	$S\left(=\frac{a}{b}\right)$
230	0.09±0.03	0^+	0	0.17±0.05	1.04
2070	0.26±0.06	2^+	1806	0.57±0.14	0.91
3160	0.06±0.01	2^+	2935	0.13±0.03	0.92

$^{(a,b)}$ Given in the present study of the reactions ^{27}Al(d,t) [vish01] and ^{27}Al(d,^{3}He) respectively. S is the spectroscopic factor only without C^2

tors reported earlier for those states which are close to the two states. The state 4847 keV is also analysed with mixing of s and d single particle orbitals. The contribution of s orbital is ≈10% of the contribution of d orbital in the extracted C^2S values. Comparison of relative C^2S value for these states with previously reported values has been given in Table. 4.6.

4.2.5 Analog states of ^{26}Al and ^{26}Mg.

Isobaric analog states (IAS) are defined as the states in the isobars with same α and isospin quantum number T but with different z component of isospin (t_z) where α defines other quantum numbers (J, π etc. including A). The spectroscopic factors of IAS should be same. In transfer reactions, isospin formalism has been taken into account by incorporating isotopic Clebsch-Gordan coefficient (C^2) in the formulation of DWBA. Since the spectroscopic factors for IAS isobaric multiplets should be identical. So, the spectroscopic factors of the low lying T=1 IAS of ^{26}Al and ^{26}Mg observed in the present study were compared. The comarison has been performed by putting the value of C^2 in the extracted C^2S values to see the effect of C^2 that how much the spectroscopic factors varries with C^2 value. The comparison is given in Table 4.7. From Table 4.7, it is clear that although the C^2S values of analog states of ^{26}Al and ^{26}Mg

are not same but the spectroscoic factor S are consistent within 11% and this inconsistency of 11% can be take care by the uncertainties in the C^2S values of the respective states. So, one can draw the conclusion from Table 4.7 that the analog states are appreciably excited. The results of the present study of IAS can be found in [vish06].

Chapter 5

Summary and Conclusions

In summary, one neutron and one proton pickup reactions ^{27}Al(d,t) and ^{27}Al(d,^{3}He) have been studied in the present thesis work with the motivation to extract spectroscopic factors of the observed states of ^{26}Al and ^{26}Mg populated through these reactions respectively. Spectroscopic factor being a fundamental property of the structure of any particular nucleus, it should be independent of reactions involved as well as energies. One of the motivation behind the study of the reaction ^{27}Al(d,t)^{26}Al was that the product nucleus ^{26}Al has recently generated a lot of interest as it is the first cosmic radioactivity detected through its characteristic gamma rays in the interstellar medium. The lifetime ($\sim 10^{6}$ y) of ^{26}Al is much shorter as compared to the time for galactic evolution ($\sim 10^{10}$ y), so the detection of ^{26}Al at the present time indicates that nucleosynthesis is currently active in our galaxy. In previous years, different reaction channels, like ^{28}Si(p,^{3}He) [Chip01], ^{28}Si(d,α) and ^{24}Mg(^{3}He,p) [Tak01], ^{27}Al(p,d) [Kro01, Shw01], ^{27}Al(^{3}He, α) [Bet01, Nur01] etc. were already used for spectroscopic study of ^{26}Al. In addition, an attempt has been made in the past to study the ^{27}Al(d,t) reaction up to 2.08 MeV excitation energy using off-line measurements of captured tritium activity in stacked ^{27}Al foils [Vla01]; however, no direct measurement of the ^{27}Al(d,t) reaction has so far been available, to the best of our knowledge, in the literature. So, the reaction ^{27}Al(d,t) was choosen to extract spectroscopic factors of

the different states of ^{26}Al with motivation to examine and compare the spectroscopic factors extracted using different reaction probes. The other nucleus of interest, ^{26}Mg, is the radioactive (β^+) decay product of ^{26}Al; so the study of ^{26}Mg, is also important in nuclear astrophysics to understand the origin of ^{26}Al. So, we chose the reaction ^{27}Al(d,^{3}He) to extract spectroscopic factors of the observed states of ^{26}Mg. Previously, the reaction (d,^{3}He) was already been studied at 29 MeV [Ver01], 34.5 MeV [Wil01], 52 MeV [Wag01] and at 80 MeV [Ard01]. So the primary motivation for the study of ^{27}Al(d,^{3}He) reaction was to examine the dependence of spectroscopic factors on optical model potential parameters used in the analysis by comparing the present results with previously reported values for the same reaction. The second motivation of the study of ^{27}Al(d,^{3}He) reaction was that to compare the spectroscopic factors for T=1 analog states in ^{26}Al and ^{26}Mg produced in (d - t/ ^{3}He) reaction sequence which is being done for the first time verification using ^{27}Al(d, t) and ^{27}Al(d,^{3}He) reactions sequence.

To fulfill the above motivation, the experiment was performed at the Variable Energy Cyclotron Centre, Kolkata using deuteron beam of energy 25 MeV on a self - supporting target ^{27}Al (90 μg/cm^2). In this experiment, we used a detector telescope system, consisting of a single - sided 55 μm thick Si (ΔE) strip detector, followed by a double - sided 1030 μm Si (E) strip detector. These two detectors were backed by four CsI(Tl) detectors (each of thickness 6 cm). The inclusive angular distributions of the ejectiles were measured in the angular range of 16° to 40° in steps of 0.9 °. Several excited states of ^{26}Al, ^{26}Mg and ^{25}Mg were produced through the reactions ^{27}Al(d, t), ^{27}Al(d, ^{3}He) and ^{27}Al(d, α). A VME based data acquisition system (DAQ) developed at VECC was used to collect the online event by event data. The offline data extraction and analysis was performed using different algorithm developed in ROOT platform.

The analysis of the data was done in two steps. In the first step, the analysis of elastically scattered deuterons from ^{27}Al target was done and then the angular distributions of the observed states of ^{26}Al and ^{26}Mg populated through the 1n and 1p transfer reactions ^{27}Al(d,t) and ^{27}Al(d,^{3}He) have been analysed to extract spectroscopic information. The elastic scattering angular distribution was used to extract

optical model potential parameters for the entrance channel using optical model code ECIS94 [Ran01]. The exit channel optical model potential parameters for both the exit channels t+^{26}Al and ^{3}He+^{26}Mg were extracted using the global parametrisation given in [Per01] and also some sets were taken from literature. In the present work, zero range distorted wave Born approximation calculation was performed using computer code DWUCK4 [kunz01] for analysis of the observed states of ^{26}Al and ^{26}Mg. The observed states of ^{26}Al were studied by assuming pick up from $0d_{5/2}$, $0g_{9/2}$ and $1s_{1/2}$ single particle orbitals. In a similar way, the observed states of ^{26}Mg were studied by assuming pick up from $0d_{5/2}$ single particle orbital but some of the states were studied assuming configuration mixing of $0d_{5/2}$ and $1s_{1/2}$ single particle orbitals.

The spectroscopic factors for the fourteen observed states of ^{26}Al populated through reaction ^{27}Al(d, t) were extracted and relative spectroscopic factors (keeping ground state spectroscopic factor to be 1) of states were compared with the previously reported values obtained using different reaction probes [Kro01, Shw01, Bet01, Nur01] as well as shell model predictions given in [Kro01, Bet01]. The spectroscopic factors for nine observed states of ^{26}Mg populated through the reaction ^{27}Al(d,^{3}He) were extracted and relative spectroscopic factors were compared with previously reported values using the same reaction [Ver01, Wil01, Wag01, Ard01] and also with predictions from the shell model given in [Wil01, Wag01] and predictions given from rotational model in [Wag01]. In the present work, T=1 analog states observed in the present study of both the reactions ^{27}Al(d,t)^{26}Al and ^{27}Al(d,^{3}He)^{26}Mg at 25 MeV were also compared by their corresponding spectroscopic factors. The result of the present work can be found in [vish01, vish02, vish03, vish04, vish05, vish06, vish07].

In summary, the results from the analysis of the reaction ^{27}Al(d,t)^{26}Al as discussed in chapter 4 may be concluded as follows; The reaction ^{27}Al(d,t) has been utilised for the first time for the study of ^{26}Al. The new sets of optical model potential parameters were extracted from d + ^{27}Al elastic scattering data. The angular distributions of different excited states of ^{26}Al were studied with the zero range distorted wave Born approximation to extract the spectroscopic factors for these states. The experi-

mental and theoretical results for both the positive and negative parity states were in good agreement with each other. The extracted values of spectroscopic factors of the observed states of ^{26}Al were found to be in good agreement with the experimental values reported earlier as well as with the respective shell model predictions whereever available. For the 420 keV state, it may be concluded that the experimental angular distribution and the corresponding DWBA prediction are in good agreement for an ℓ = 2 transfer, while it is not so for an ℓ = 0 transfer. It was earlier indicated that this state was populated with pure ℓ = 0 transfer [Kro01, Bet01]. However, from the present study we conclude that it resembles more closely with an ℓ = 2 transfer, rather than an ℓ = 0 transfer. Interestingly, the spectroscopic factor obtained from the present study is comparable with its previously reported value for ℓ = 0 transfer as well as the respective theoretical predictions [Kro01]. The potential parameter dependence of spectroscopic factors was checked with two different sets of exit channel potential parameters. It was found that for the ^{27}Al(d,t) reaction at 25 MeV, the variation in spectroscopic factors was less than 10%. The estimated uncertainties in the extracted values of spectroscopic factors are within 30% except for the states at 420 keV (ℓ = 0 case) and 3505 keV (ℓ = 4 case). The present results also compare well with the previous measurements.

The results from the analysis of the reaction ^{27}Al(d,^{3}He)^{26}Mg as discussed in chapter 4 may be concluded as follows; different excited states of ^{26}Mg were studied with zero range distorted wave Born approximation using the reaction ^{27}Al(d, ^{3}He)^{26}Mg at 25 MeV beam energy. The experimental data was found to be well reproduced by the theoretical predictions. The extracted values of spectroscopic factors were found to be in good agreement with those reported earlier and were also found in agreement with the predictions from shell model and rotational model. The extracted C^2S values for the analog states of ^{26}Al and ^{26}Mg were studied and were found to be in good agreement indicating that the ratios of the production of analogs were equally probable. The variation between analog states is an important issue for deriving resonance strength in nuclear astrophysics. Two sets of exit channel potential parameters were used to check the variation in the extracted spectroscopic factors for the observed states of ^{26}Mg. In

the present study of the reaction ^{27}Al(d,^{3}He), less than 25% variation has been observed in extracted C^2S values of the states of ^{26}Mg for ℓ= 2 transfer between the two combination of entrance-exit channel potential parameters while for ℓ= 0 contribution, the variation was in the range between 10 to 67%. It has also been verified that the change in the radius of bound-state potential affected the C^2S value significantly and reduces the the extracted C^2S values up to 25% for ℓ= 2 transfer while for ℓ= 0 transfer, it has decreased upto 40%. All those factors that affected C^2S values, which have been discussed in the present study, were used to estimate the uncertainties in the extracted C^2S values. It was found that the variation in the estimated uncertainties in the extracted C^2S were 10 to 36%.

In conclusion, both the reactions ^{27}Al(d,t)^{26}Al and ^{27}Al(d,^{3}He)^{26}Mg were found to be good probe to study different states of ^{26}Al and ^{26}Mg. The experimental data was found to be well reproduced by the theoretical predictions. The experimentally extracted spectroscopic factors were found to be in good agreement with the theoretical predictions from different model codes and also with those reported earlier.

The present study showed that all available sets of optical model parameters may not be equally suitable for fitting the angular distributions of the reaction products (and, therefore, for the extraction of spectroscopic factors). This may be due to the inherent limitations (range, precision, quality of fitting, etc.) associated with the particular sets of data as well as the analysis techniques. So, it will also be interesting to have a systematic study of optical model potential parameters for both entrance (d +^{27}Al) and exit (inverse : closest possible) channels (say, ^{3}He + ^{27}Al, in place of ^{3}He + ^{26}Mg) alongwith the transfer study; this will certainly minimise the uncertainties due to variations of systematic errors in different experimental/analysis procedures. This is likely to help reduce the variation in extracted spectroscopic factors studied using different channels. The present study also indicated that the one nucleon (p/n) transfer may also be used for study of isobaric analog states (IAS) in isobaric multiplets.

Bibliography

[Alm01] S. Almaraz-Calderon *et al*., Phys. Rev. Lett. **112**, 152701(2014).

[Ard01] M. Arditi *et al*., Nucl. Phys. A **165**, 129(1969).

[Ber01] Nuclear Reactions by C. A. Bertulani, arXiv:0908.3275v2 [nucl-th] 14 Jul 2010.

[Biz01] M. Bizzarro, J. A. Baker and H. Haack *et al*., Nature(London) **431**, 275 (2004).

[Bet01] R. R. Betts, *et al*., Phys. Rev. C **8**, 670 (1973).

[Burl01] M. Burlein *et al*., Phys. Rev. C **29**, 2013 (1984).

[Bas01] W. W. Daehnick *et al*., Phys. Rev. **149**, 791 (1977).

[Chip01] K. A. Chipps *et al*., Phys. Rev. C **86**, 014329 (2012).

[Dieh01] R. Diehl *et al*., Nature(London) **439**, 45 (2006).

[Div01] A. S. Divatia, Eighth International Conference on Cyclotron and their application, Bloominton, Indiana (1978).

[End01] P. M. Endt *et al*., Nucl. Phys. A **633**, 1 (1998).

[End02] P. M. Endt *et al*., Nucl. Phys. A **487**, 221 (1988).

[End03] P. M. Endt *et al*., Nucl. Phys. A **476**, 333 (1988).

[End04] P. M. Endt *et al*., Nucl. Phys. A **521**, 1 (1990).

[End05] P. M. Endt, Atomic Data and Nuclear Data tables, **19**, 23(1977).

[Fit01] C. Fitoussi *et al*., Phys. Rev. C **78**, 044613 (2008).

[Fin01] P. Finlay *et al*., Phys. Rev. Lett. **106**, 032501(2011).

[Gsh01] S.N. Ghoshal, Nuclear Physics, S. chand & company limited (ISBN: 81-219-0413-7).

[Gle01] Norman K Glendenning, Direct Nuclear Reactions, World Scientific Publishing,2004.

[Hyd01] K Heyde, Basic Ideas and concepts in nuclear physics, Third Edition;An Introductory approach(ISBN:978-0-7503-0980-6).

[Hop01] Hoppe, P., Amari, S., Zinner, E., Ireland, T., and Lewis, R. S. 1994, ApJ, 430, 870.

[Hus01] Huss, G. R., Hutcheon, I. D. and Wasserburg, G. J. 1997, Geochim. Cosmochim. Acta, 61, 5117.

[Herm01] H. Feshbach, C. E. Porter and V. F. Weisskopf, Phys.Rev. 90, 166 (1953).

[Her01] W. R. Hering *et al*., Nucl. Phys. A **151**, 33(1970).

[JKra01] J. J. Kraushaar *et al*., Phys. Rev. C **34**, 1530 (1986).

[kunz01] http://spot.colorado.edu/ kunz/DWBA.html.

[Kra01] K.S. Krane. Introductory Nuclear Physics. John Wiley & Sons, 1987(ISBN:978-81-265-1785-5).

[Kro01] J. Kroon *et al*., Nucl. Phys. A **204**, 609 (1973).

[Knoll] Text book; Radiation Detection and Measurement by Glenn E Knoll.

[Lee01] J. Lee *et al.*, Phys. Rev. C **79**, 054611 (2009).

[Lee02] http://www.phy.cuhk.edu.hk/internship/sure/comments_2004/*lhc*_rep.pdf.

[LeoWR] Techniques for Nuclear and Particle Physics Experiments by William R Leo.

[LISE] *http* : //*lise.nscl.msu.edu*/*lise.html.*

[Mah01] J. B. Maher *et al.*, Phys. Rev. C **5**, 1313 (1972).

[Pal01] Theory of nuclear structure by M. K. Pal, (EWP) Affiliated East-West Press Pvt Ltd, New Delhi(ISBN:81-85336-81-4).

[Nur01] J. Nurzynski *et al.*, Nucl. phys. A **107**, 581 (1968).

[Nnd02] http://www.nndc.bnl.gov/chart/getdataset.jsp?nucleus=26MG&unc=nds.

[Nnd01] http://www.nndc.bnl.gov/nudat2/adopted_searchi.jsp.

[Pbh01] Structure of the Nucleus by M A Preston and R K bhaduri.

[Pran01] N. Prantzos *et al.*, Phys. Rep. **267**, 1 (1996).

[Phe01] MacPherson, G. J., Davies, A. M. and Zinner, E. K. 1995, Meteoritics, 30, 365

[Per01] C. M. Perey and F. G. Perey *et al.*, Atomic Data and Nuclear Data Tables **17** , l (1976).

[Ren01] Nuclear Reactions with Heavy Ions by Reiner Bass, Springer-Verlag Berlin Heidelberg New York 1980.

[Ran01] J. Raynal, Notes on ECIS94, NEA 0850/16.

[Sit01] Theory of nuclear reactions by A G Sitenko, World Scientific Publishing Co. Pte. Ltd (ISBN: 9971-50-481-2).

[Sat01] G. R. Satchler, Rev. Mod. Phys. , Vol. 50, No. 1, Part I, January 1978.

[Sat02] Direct Nuclear Reactions By G. R. Satchler, Clarendon Press-Oxford,Oxford University Press-New York, 1983.

[Sat03] G. R. Satchler, Nucl. Phys. , 55, (1964)1-33.

[Sat04] W. Satula, J. Dobaczewski, W. Nazarewicz and R. Rafalski *al*., Phys. Rev. Lett. **106**, 132502(2011).

[SRIM] James F. Ziegler, *SRIM2008*, *http* : //*www.srim.org*/*SRIM*/*SRIM2008.pdf*.

[Shw01] D. L. Show *et al*., Nucl. Phys. A **263**, 293 (1976).

[Tak01] N. Takahashi *et al*., Phys. Rev. C **23**, 1305 (1981).

[Tsa01] M. B. Tsang, Jenny Lee and W. G. Lynch *al*., Phys. Rev. Lett. **95**, 222501 (2005).

[TK01] Thesis on the Study of the hoyle state by Tapan Kumar Rana(Private Communication).

[Trib01] R. E. Tribble *et al*., Nucl. Phys. A **282**, 269(1977).

[Uda01] T. Udagawa, Y. J. Lee, and T. Tamura *al*., Phys. Rev. C **39**, 47 (1989).

[Vla01] N A Vlasov, S P Kahnm, A A Ogloblln and V I Chuev, JETP (Sov Phys) 37 (1960) 844.

[Ver01] J. Vernotte *et al*., Phys. Rev. C **48**, 205 (1993).

[vish01] Vishal Srivastava *et al*., Phys. Rev. C **91**, 054611 (2015).

[vish02] Vishal Srivastava *et al.*, EPJ Web of Conferences **86**, 00055 (2015).

[vish03] Vishal Srivastava *et al.*, Proceedings of the DAE Symp. on Nucl. Phys. 59, 358 (2014).

[vish04] Vishal Srivastava *et al*., Proceedings of NN2015 to be published in EPJ web of conf.

[vish05] Vishal Srivastava *et al.*, arXiv:1510.04416.(Under Review in Phys. Rev. C).

[vish06] Vishal Srivastava *et al.*, Phys. Rev. C **93**, 044601 (2016).

[vish07] Vishal Srivastava *et al.,* Proceedings of the DAE Symp. on Nucl. Phys. 60, 342 (2015).

[Wass01] G. J. Wasserburg *et al*., Nucl. Phys. A **777**, 5 (2006).

[Wil01] B. H. Wildenthal *et al*., Phys. Rev. **175**, 1431 (1968).

[Wag01] G. J. Wagner *et al*., Nucl. Phys. A **125**, 80(1969).

[Yas03] M. Yassue *et al*., Phys. Rev. C **42**, 1279 (1990).

[UK01] Micronsemiconductor limited, Royal buildings, Marlborough road, Lancing, Sussex, BN 158UN, England.